Title

ANKRD16 prevents neuron loss caused by an editing-defective tRNA synthetase.

Journal

Nature, 557(7706)

ISSN

0028-0836

Authors

Vo, My-Nuong
Terrey, Markus
Lee, Jeong Woong
et al.

Publication Date

2018-05-01

DOI

10.1038/s41586-018-0137-8

Peer reviewed

HHS Public Access

Author manuscript

Nature. Author manuscript; available in PMC 2018 November 16.

Published in final edited form as:

Nature. 2018 May ; 557(7706): 510–515. doi:10.1038/s41586-018-0137-8.

ANKRD16 prevents neuron loss caused by an editing-defective tRNA synthetase

My-Nuong Vo[*,1], **Markus Terrey**[*,2,3], **Jeong Woong Lee**[4], **Bappaditya Roy**[5], **James J. Moresco**[6], **Litao Sun**[1], **Hongjun Fu**[7], **Qi Liu**[8], **Thomas G. Weber**[9], **John R. Yates III**[10], **Kurt Fredrick**[5], **Paul Schimmel**[11,§], and **Susan L. Ackerman**[2,3,§]

[1]The Skaggs Institute for Chemical Biology, Scripps Research Institute, La Jolla, CA 92037, USA

[2]Howard Hughes Medical Institute, Department of Cellular and Molecular Medicine, University of California San Diego, Medical School and Section of Neurobiology, University of California San Diego, La Jolla, CA 92093, USA

[3]Graduate School of Biomedical Sciences and Engineering, University of Maine, Orono, ME 04469, USA

[4]The Jackson Laboratory, Bar Harbor, ME 04609, USA

[5]Department of Microbiology, Center for RNA Biology, The Ohio State University, Columbus, OH 43210, USA

[6]Department of Chemical Physiology, Scripps Research Institute, La Jolla, CA 92037, USA

[7]The Jackson Laboratory, Bar Harbor, ME 04609, USA

[8]Ohio State Biochemistry Program, Department of Microbiology, and Center for RNA Biology, The Ohio State University, Columbus, OH 43210

[9]Dynamic Biosensors GmbH, 82152 Martinsried, Germany

[10]Department of Chemical Physiology, Scripps Research Institute, La Jolla, CA 92037, USA

[11]The Skaggs Institute for Chemical Biology, The Scripps Research Institute, La Jolla, CA 92037, USA; and The Scripps Research Institute, Jupiter, FL 33458, USA

Correspondence and requests for materials should be addressed to S.L.A. (sackerman@ucsd.edu) or P.S. (schimmel@scripps.edu).
Jeong Woong Lee, Current Address: Korea Research Institute of Bioscience and Biotechnology, Yusung, 34141, Daejeon, South Korea
James J. Moresco, Current Address: Salk Institute for Biological Studies, La Jolla, CA 92037, USA
Hongjun Fu, Current Address: Department of Pathology and Cell Biology, Taub Institute for Research on Alzheimer's Disease and the Aging Brain, Columbia University Medical Center, New York, NY 10032, USA
Qi Liu, Current Address: *Sharklet* Technologies, Aurora, CO 80045, USA
[*]These authors contributed equally to this work.
[§]These authors jointly supervised this work.

Supplementary Information is available in the online version of the paper.

Author Contributions S.L.A., K.F., P.S., M.T., and M-N.V. designed experiments and wrote the paper. M.T., J-W.L., and H.F. performed mouse and cell culture experiments, M-N.V., L.S. and T.G.W. performed biochemical experiments, B.R. and Q.L. performed di-peptide experiments, and J.J.M. performed the mass spectrometry under J.Y.'s guidance.

The authors declare no competing financial interests.

Abstract

Editing domains of aminoacyl tRNA synthetases correct tRNA charging errors to maintain translational fidelity. A mutation in the editing domain of alanyl tRNA synthetase (AlaRS) in *Aars*^{sti} mutant mice resulted in an increased production of serine-mischarged tRNA^{Ala} and degeneration of cerebellar Purkinje cells. By positional cloning, we identified *Ankrd16,* which acts epistatically with the *Aars*^{sti} mutation to attenuate neurodegeneration. ANKRD16, a vertebrate-specific, ankyrin repeat-containing protein, binds directly to the catalytic domain of AlaRS. Serine misactivated by AlaRS is captured by lysine side chains of ANKRD16, preventing the charging of serine adenylates to tRNA^{Ala} and precluding serine misincorporation in nascent peptides. Deletion of *Ankrd16* in the *Aars*$^{sti/sti}$ brain causes widespread protein aggregation and neuron loss. These results identify a novel amino acid-accepting co-regulator of tRNA synthetase editing as a new layer of the machinery essential for preventing severe pathologies that arise from defects in editing.

Accurate aminoacylation of tRNAs by tRNA synthetases establishes the universal genetic code and occurs in two steps: first, activation of the selected amino acid with ATP to form an aminoacyl adenylate; second, transfer of the aminoacyl group of the adenylate to the 2’- or 3’-OH of the cognate tRNA. However, structural similarities between some amino acids allow misactivation of non-cognate amino acids and subsequent misacylation of tRNA. These errors can be corrected by the hydrolytic editing functions found in many tRNA synthetases [1, 2]. ‘Editing’ can occur after amino acid misactivation, but prior to aminoacyl transfer, or after aminoacylation of tRNA, known as pre-transfer and post-transfer editing, respectively. Pre-transfer editing occurs in either the aminoacylation active site or in a distinct editing site, whereas post-transfer editing occurs only in the editing site of these enzymes [3, 4, 5].

The importance of tRNA synthetase editing including editing by the alanyl tRNA synthetase (*Aars*; AlaRS) has been shown in multiple organisms [6, 7, 8, 9, 10, 11]. Although AlaRS misactivates both glycine and serine, misactivation of serine appears to have more serious consequences, perhaps due to the presence of D-aminoacyl-tRNA deacylases which act on Gly-tRNA^{Ala} [12, 13, 14]. We previously showed that sticky (*sti*) mutant mice that have a point mutation (Ala734Glu) in the editing domain of AlaRS have ubiquitinated protein aggregates in cerebellar Purkinje cells and subsequent degeneration of these neurons [9]. The *sti* mutation results in only a 2-fold increase in the generation of Ser-tRNA^{Ala}, demonstrating that Purkinje cells are particularly sensitive to loss of AlaRS editing [9].

Here we identified a novel vertebrate-specific gene *Ankrd16* that greatly attenuates misfolded aggregate formation and Purkinje cell degeneration in *Aars*$^{sti/sti}$ mice. Deletion of *Ankrd16* in other *Aars*$^{sti/sti}$ neurons also caused formation of ubiquitinated protein aggregates and neuron death. ANKRD16 binds to AlaRS and prevents misincorporation of serine at alanine codons in nascent peptides by stimulating serine-dependent ATP hydrolysis prior to tRNA aminoacylation via acceptance of misactivated serines. Our data collectively reveal ANKRD16 as a co-regulator of AlaRS that protects against assaults on translation fidelity and proteostasis in mammalian neurons.

Results

Ankrd16 suppresses *Aars*^{sti}-mediated Purkinje cell degeneration

Aars$^{sti/sti}$ mice on the inbred C57BL/6J (B6) genetic background are ataxic with cerebellar Purkinje cell degeneration beginning at 3 weeks of age [9]. However, neither ataxia nor Purkinje cell degeneration was apparent in 9/10 F2 *Aars*$^{sti/sti}$ mice from a B6.*Aars*$^{sti/+}$ and CAST/Ei (CAST) mating at 12–16 months old, suggesting that CAST-derived alleles could suppress neuron loss. In agreement, two phenotypically distinct classes of N1 *Aars*$^{sti/sti}$ offspring (generated from a backcross of F1 B6/CAST *Aars*$^{sti/sti}$ mice to B6.*Aars*$^{sti/+}$ mice) were observed at equal frequencies: mice with ataxia and extensive Purkinje cell loss similar to that of B6.*Aars*$^{sti/sti}$ mice and mice without ataxia and little Purkinje cell loss (Extended Data Fig. 1a). Suppression of the neurodegenerative phenotype was observed in 50% of backcross mice from crosses to CASA/RkJ (CASA; a strain closely related to CAST/Ei), but not in other crosses, suggesting that a single dominant allele from the CAST or CASA strains can suppress *sti*-mediated neurodegeneration (Extended Data Fig. 1a).

Genome scans on affected and unaffected N1 *Aars*$^{sti/sti}$ mice revealed that the Purkinje cell degeneration was suppressed in mice that were heterozygous for CAST alleles on proximal Chromosome 2 (Extended Data Fig. 1b). This locus (~3.3Mbp) also segregated with the *Aars*$^{sti/sti}$ modifier gene from CASA, suggesting these strains share the same suppressor gene. Transfer of the *M*odifier of *sti*cky (*Msti*) locus from the CAST genome onto the B6.*Aars*$^{sti/sti}$ genetic background rescued the decreased latency to fall in a rotorod test of 3-month-old B6.*Aars*$^{sti/sti}$ mice and dramatically reduced Purkinje cell death, although some neurons in the rostral cerebellum of these mice still degenerated (Fig. 1a, 1b). Heterozygosity and homozygosity for CAST alleles in the *Msti* region similarly attenuated Purkinje cell loss, in agreement with the dominant nature of *Msti* (Fig. 1b).

Ubiquitin punctae characteristic of protein inclusions were observed in many Purkinje cells in 4-week-old B6.*Aars*$^{sti/sti}$, but not in B6 or CAST, mice (data not shown). As expected due to progressive Purkinje cell loss observed in *sti* mutant mice, the number of Purkinje cells containing inclusions decreased by 6 and 12 weeks of age. However, very few Purkinje cells in B6.*Msti*$^{CAST/B6}$; *Aars*$^{sti/sti}$ mice contained inclusions, even at later ages, confirming long-term protection of Purkinje cells (Fig. 1c).

We further localized *Msti* to a 0.63 Mbp region and the coding regions of the protein-coding genes in this interval were amplified by RT-PCR from B6 and CAST cerebellar RNA and sequenced (Fig. 2a). Non-synonymous SNPs were observed in *Il2rα, Fbxo18*, and *Ankrd16* (Fig. 2a). However, with the exception of *Il2rα*, these SNPs were either not present in CASA, an *Aars*$^{sti/sti}$ modifying strain (*Fbxo18*), or were also present in MOLF (*Ankrd16*), a strain in which neurodegeneration is not rescued (Extended Data Fig. 1a and 1c).

A strain-specific *Ankrd16* transcript that contained a 138 bp cryptic exon (exon 5') was also observed in B6 (with or without the *Aars*$^{sti/sti}$ mutation) and other non-rescuing strains, but was absent in CAST or CASA (Fig. 2b, Extended Data Fig. 1d and e). Sequence analysis of intron 5 suggested that inclusion of this exon was due to a SNP that generated a novel alternative splice site (Fig. 2c, Extended Data Fig. 1f). Transcript levels of the correctly

spliced *Ankrd16* isoform (lacking exon 5') were 3.3 and 5.3 fold higher in the congenic *Msti*$^{CAST/B6}$ or CAST cerebellum relative to B6, respectively (Fig. 2d). Protein levels were 2.8 ± 0.2 and 3.9 ± 0.22 fold higher in the B6.*Msti*$^{CAST/B6}$ and CAST cerebellum, respectively, and the *Aars*$^{sti/sti}$ mutation did not alter *Ankrd16* splicing or protein levels (Fig. 2e, Extended Data Fig 1e and g). Increased ANKRD16 levels were also observed in other tissues from *Msti*$^{CAST/B6}$ mice (Extended Data Fig. 1h). The *Ankrd16* transcript with exon 5' contains a premature stop codon and is predicted to undergo nonsense-mediated decay and in agreement, truncated forms of ANKRD16 were not observed (Fig. 2e, Extended Data Fig. 1g).

Neurodegeneration in *Aars*$^{sti/sti}$ mice was modified neither by transgenic expression of the CAST *Il2rα* cDNA nor deletion of *Il2rα* (data not shown). However, suppression of *Aars*$^{sti/sti}$-mediated Purkinje cell loss was observed in mutant mice that carried a CAST BAC transgene containing the 3'portion of the *Il15rα* gene, and the *Fbxo18* and *Ankrd16* genes (Fig. 2f). However, another transgenic line (Tg*25L9-19*) generated with this BAC in which *Ankrd16* was deleted upon integration was not able to suppress Purkinje cell degeneration (Fig. 2f, Extended Data Fig. 1i). Indeed, transgenic expression of the *Ankrd16*^{CAST} coding sequence using the Purkinje cell-specific promoter *Pcp2* in B6.*Aars*$^{sti/sti}$ mice suppressed the death of these neurons (Fig. 2g).

ANKRD16 binds AlaRS to reduce misincorporation of serine

ANKRD16 encodes a 39 kDa protein of unknown function that is composed of nine repeats of the ankyrin protein-protein interaction domain and is found only in vertebrates (Extended Data Fig. 2a, Extended Data Fig. 1j). To identify proteins that interact with ANKRD16, we transgenically expressed *Ankrd16-myc* under the control of the chicken beta-actin promoter and cytomegalovirus enhancer [15, 16]. Co-immunoprecipitation (Co-IP) of ANKRD16 was performed using livers of transgenic and non-transgenic mice, and the immunoprecipitates were analyzed via tandem mass spectrometry (LC-MS/MS). Surprisingly, AlaRS was the most abundant protein after the ANKRD16 bait protein (Extended Data Fig. 2a). Interaction of ANKRD16 with wild type or mutant AlaRS in the liver and brain was confirmed by Co-IP/western blotting (data not shown and Fig. 3a). Interactions between ANKRD16 and AlaRS were independent of both the epitope tag and bait protein (Extended Data Fig. 2b and c).

Co-IP experiments demonstrated that the AlaRS aminoacylation domain was efficiently co-immunoprecipitated by ANKRD16, and little interaction was observed in the absence of this domain (Fig. 3b, Extended Data Fig. 2b). Affinity-capture experiments using purified AlaRS protein further defined that the AlaRS catalytic domain was sufficient for ANKRD16 interaction and that this interaction was direct (Extended Data Fig. 2e, Fig. 3c). Furthermore, AlaRS did not Co-IP ANKRD29, a protein comprised of 8 ankyrin repeats (Extended Data Fig. 2d), nor did ANKRD16 interact with tyrosyl-tRNA synthetase or tryptophanyl-tRNA synthetase (Fig. 3c), suggesting a specific ANKRD16-AlaRS interaction with similar binding dynamics between AlaRS^{WT} and AlaRS^{A734E} (Extended Data Fig. 2f).

The AlaRS^{A734E} mutation leads to increased death of *Aars*$^{sti/sti}$ embryonic fibroblasts when cultured with increasing concentrations of serine [9]. *Msti*$^{CAST/B6}$; *Aars*$^{sti/sti}$ fibroblasts were

more resistant than B6.*Aars*$^{sti/sti}$ fibroblasts to high serine concentrations, and at the highest concentrations (40 mM), less cell death was observed in *Msti*$^{CAST/B6}$; *Aars*$^{sti/sti}$ than in B6 (*Msti*$^{B6/B6}$) fibroblasts demonstrating that *Ankrd16* suppresses serine-mediated cell death in *Aars*$^{sti/sti}$ cells (Fig. 3d)

Although ANKRD16 is a vertebrate-specific gene, mammalian and *E. coli* AlaRS are highly conserved with ~67% similarity in the catalytic domain. Indeed, mouse ANKRD16 was able to affinity-capture *E. coli* AlaRS (Fig. 3c), and reduced death of *E. coli* with a severe editing domain mutation (C666A/Q584H) in AlaRS when grown on a serine gradient (Fig. 3e). Together, these results suggest that ANKRD16 influences AlaRS function.

Next, we used dipeptide formation on defined ribosome complexes as a read-out of charging and decoding fidelity. These experiments sufficiently detected serine mistranslation and AlaRS-mediated editing of Ser-tRNA^{Ala} (Extended Data Fig. 3a and b). When reactions using Ser-tRNA^{Ala} and AlaRS were supplemented with alanine, loss of fMet-Ser coincided with gain of fMet-Ala (Fig. 4a), consistent with reported post-transfer editing by AlaRS [7]. However, no obvious differences were observed between reactions using AlaRS^{WT} or AlaRS^{A734E}, and ANKRD16 had no effect on either reaction in these experiments using mischarged tRNA.

In contrast, when deacyl tRNA^{Ala}, serine, and ATP were used, AlaRS^{A734E} generated more fMet-Ser than AlaRS^{WT} and ANKRD16 reduced the amount of this aberrant dipeptide in reactions with either AlaRS^{A734E} or AlaRS^{WT} (Extended Data Fig. 3c). Although ANKRD16 interacts with AlaRS$^{1–455}$ (Extended Data Fig. 2f), no reduction in the amount of aberrant dipeptide was observed, implying the editing and/or C-terminal domains of AlaRS may contribute to ANKRD16 function. Furthermore, in the presence of ATP and a mixture of Ser and Ala, ANKRD16 specifically decreased fMet-Ser formation, thereby increasing AlaRS^{A734E} fidelity (i.e., fMet-Ala/fMet-Ser) by a factor of ~20 (Fig. 4b). Thus, ANKRD16 acts prior to formation of mischarged tRNA to enhance translational fidelity.

In agreement, ANKRD16 had no effect on subsequent steps of tRNA mischarging including deacylation of mischarged Ser-tRNA^{Ala}, transfer of the mischarged tRNA to EF-Tu, or activation/aminoacylation of the cognate amino acid alanine (Extended Data Fig. 3d–g). In addition to post-transfer editing activity, in *E. coli* pre-transfer editing has also been observed in AlaRS [17]. Serine-dependent ATPase activity was also observed with mouse AlaRS^{WT} in the absence of tRNA (Extended Data Fig. 4a). However, this activity was decreased with both AlaRS^{A734E} and AlaRS$^{1–455}$ (Fig. 4c, Extended Data Fig. 4b). ANKRD16 was able to restore that activity for AlaRS^{A734E}, but not for AlaRS$^{1–455}$, further suggesting that the editing domain contributes to the serine-dependent ATPase activity and/or the modulation of this activity by ANKRD16 (Fig. 4c, Extended Data Fig. 4b and c).

Unexpectedly, ANKRD16 appeared to stimulate tRNA-dependent precipitation of ^{3}H-serine but not of ^{3}H-alanine in reactions with AlaRS^{A734E} (Extended Data Fig. 4d–f). However, misactivated ^{3}H-serine was also precipitated in reactions without tRNA^{Ala} with approximately three linked-serine adducts per ANKRD16 (Extended Data Fig. 4g). In contrast, ^{3}H-alanine-adduct formation per ANKRD16 with AlaRS^{A734E}, in the absence of

tRNA^{Ala}, was much lower (Extended Data Fig. 4h). Furthermore, in the presence of tRNA^{Ala} and AlaRS^{A734E}, alanine linked to ANKRD16 was negligible relative to that coupled to tRNA^{Ala} (Fig. 4d).

These results suggest that ANKRD16 functions as an alternative to water or tRNA^{Ala}, accepting misactivated serine. Previous studies have demonstrated that reactive aminoacyl adenylates may react with cysteine or lysine residues [18, 19, 20, 21]. Levels of precipitated serine were only slightly diminished after prolonged exposure to alkaline pH, which hydrolyzes thiol esters (e.g. cysteine). Thus, the ANKRD16 serine adduct is likely an amide (e.g. lysine) (Extended Data Fig. 4i).

To identify residues of ANKRD16 that accept misactivated serine, we utilized mass spectrometry. No spectral shift with Cys-containing peptides was observed. While not all Lys-containing peptides of ANKRD16 were resolved, highly conserved lysines - K102, K135, and K165 - shifted by 87 Da (the mass of serine) (Extended Data Fig. 1j, Extended Data Fig. 5a–d). Therefore, we mutated those Lys codons to Arg (ANKRD16^{3xArg}) (Extended Data Fig. 4g). Circular dichroism spectroscopy and thermal shift assays suggested that wild type and ANKRD16^{3xArg} have similar secondary structures and stabilities (Extended Data Fig. 5e and f), and only a slight change (~2 fold) in affinity for AlaRS^{A734E} (Extended Data Fig. 2f and 5g). In contrast to ANKRD16, ANKRD16^{3xArg} had no effect on AlaRS^{A734E} pre-transfer editing (Fig 4e, Extended Data Fig. 4b). Unlike ANKRD16, which rescued AlaRS$^{C666A/Q584H}$. *E. coli* growth in high levels of serine, ANKRD16^{3xArg} did not rescue growth of mutant bacteria under these conditions (Fig. 4f). Similarly, serine-induced death of B6.*Aars*$^{sti/sti}$ embryonic fibroblasts was prevented by expression of *Ankrd16*, but not *Ankrd16*^{3xArg} (Fig. 4g, Extended Data Fig. 6). Accordingly, we generated a model for the ANKRD16-AlaRS complex (Fig. 4h). Modified lysine side chains of ANKRD16 project out from the helix-loop-helix motifs, with each in close proximity to the active site of AlaRS, where serine is misactivated.

Complete loss of *Ankrd16* in *Aars*$^{sti/sti}$ mice leads to extensive neurodegeneration

To determine if the specificity of neuron death in *Aars*$^{sti/sti}$ mice is correlated with the ANKRD16 levels, we performed immunofluorescence. ANKRD16 was widely expressed in the brain and was detected in the nucleus as well as the cytoplasm (Fig. 5a, Extended Data Fig. 7a, b). Intriguingly, ANKRD16 levels were lower in Purkinje cells relative to cerebellar granule cells, cells of the cerebellar molecular layer, hippocampal neurons, and cells in the cortex (Fig. 5a).

To test if the levels of *Ankrd16* influence the sensitivity of cells to the *Aars*$^{sti/sti}$ mutation, we generated an *Ankrd16* null allele (Extended Data Fig. 7c, d). *Ankrd16*$^{-/-}$ mutant mice had no obvious pathologies in the brain or other organs, even when aged to 12 months (data not shown). However, loss of *Ankrd16* in *Aars*$^{sti/sti}$ mice resulted in early embryonic lethality (Extended Data Fig. 7e). These results show that the low levels of ANKRD16 present in B6 mice are sufficient to resolve *sti*-mediated editing defects induced during embryonic development.

To determine the impact of decreasing ANKRD16 levels on neuronal cell survival we conditionally deleted *Ankrd16* in postnatal Purkinje cells in *Aars*$^{sti/sti}$ mice. Purkinje cell loss in B6.Pcp2-Cre; *Ankrd16*$^{fl/-}$; *Aars*$^{sti/sti}$ mice began at about 3 weeks of age; by 4 weeks of age, the majority of Purkinje cells were absent and in contrast to *Aars*$^{sti/sti}$ mice, all Purkinje cells had degenerated by 7 months of age (Extended Data Fig. 8a and Extended Data Fig. 9a). Formation of ubiquitin- and p62-positive aggregates was also accelerated in Purkinje cells with aggregates observed in 12.3% of Purkinje cells compared to 2.5% of these neurons in *Aars*$^{sti/sti}$ mice at 3-weeks of age (Extended Data Fig. 9a).

Deletion of *Ankrd16* in the embryonic cerebellar primordium using *En1*-Cre [22] resulted in protein aggregates and neuron death in interneurons in the molecular layer and neurons in the granule cell layer in addition to Purkinje cells (Extended Data Fig. 8b, 8c, and 9b). Furthermore, loss of *Ankrd16* in postnatal cortical and hippocampal neurons also caused their degeneration. Ubiquitin- and p62-positive aggregates were observed both in hippocampal pyramidal cells (2.80% ± 0.22%) and cortical neurons in 2-month-old B6.*CaMKIIa*-Cre; *Ankrd16*$^{fl/-}$; *Aars*$^{sti/sti}$ mice (Fig. 5b–d, Extended Data Fig. 9c). Together, these data demonstrate that neurons other than Purkinje cells are also sensitive to the effects of mistranslation and further suggest that ANKRD16 protects against mistranslation in a dose-dependent fashion.

Discussion

In contrast to known editing mechanisms of tRNA synthetases or free-standing homologs of editing domains that act autonomously [23, 24], tRNA-independent hydrolysis of misactivated serine by AlaRS is enhanced through binding of ANKRD16 which captures misactivated serine and removes it from the pool for protein synthesis (Extended Data Fig. 10a and b). Unlike most tRNA synthetases, AlaRS not only misactivates smaller (glycine) but also larger (serine) amino acids than alanine due to structural properties that make it difficult for AlaRS to exclude misactivated serine [2, 24, 25, 26, 27]. Thus, serine misactivation by AlaRS, and the toxic effects of Ser-for-Ala replacements in vertebrates, may present a special situation in which an editing co-factor is necessary for proofreading.

In addition to providing direct mechanistic insights into editing functions of aminoacyl tRNA synthetases, the discovery of *Ankrd16* highlights the importance of studing mRNA translation in higher organism and may provide understanding for the cell-type sensitivity of phenotypes associated with the *Aars*^{sti} mutation. More broadly, cell-type selectivity resulting from “monogenic” mutations in ubiquitous genes has been difficult to resolve. Only a few modifier genes of disease mutations have been identified in an unbiased approach and these suggest that modifier genes may function in independent, parallel pathways [28, 29, 30]. Our identification of *Ankrd16* as a modifier of the *Aars*^{sti} mutation demonstrates that this possibility may be an oversimplification and that restricted pathologies may be due to the expression levels of genes that modify the function of the gene harboring the primary mutation.

Extended Data

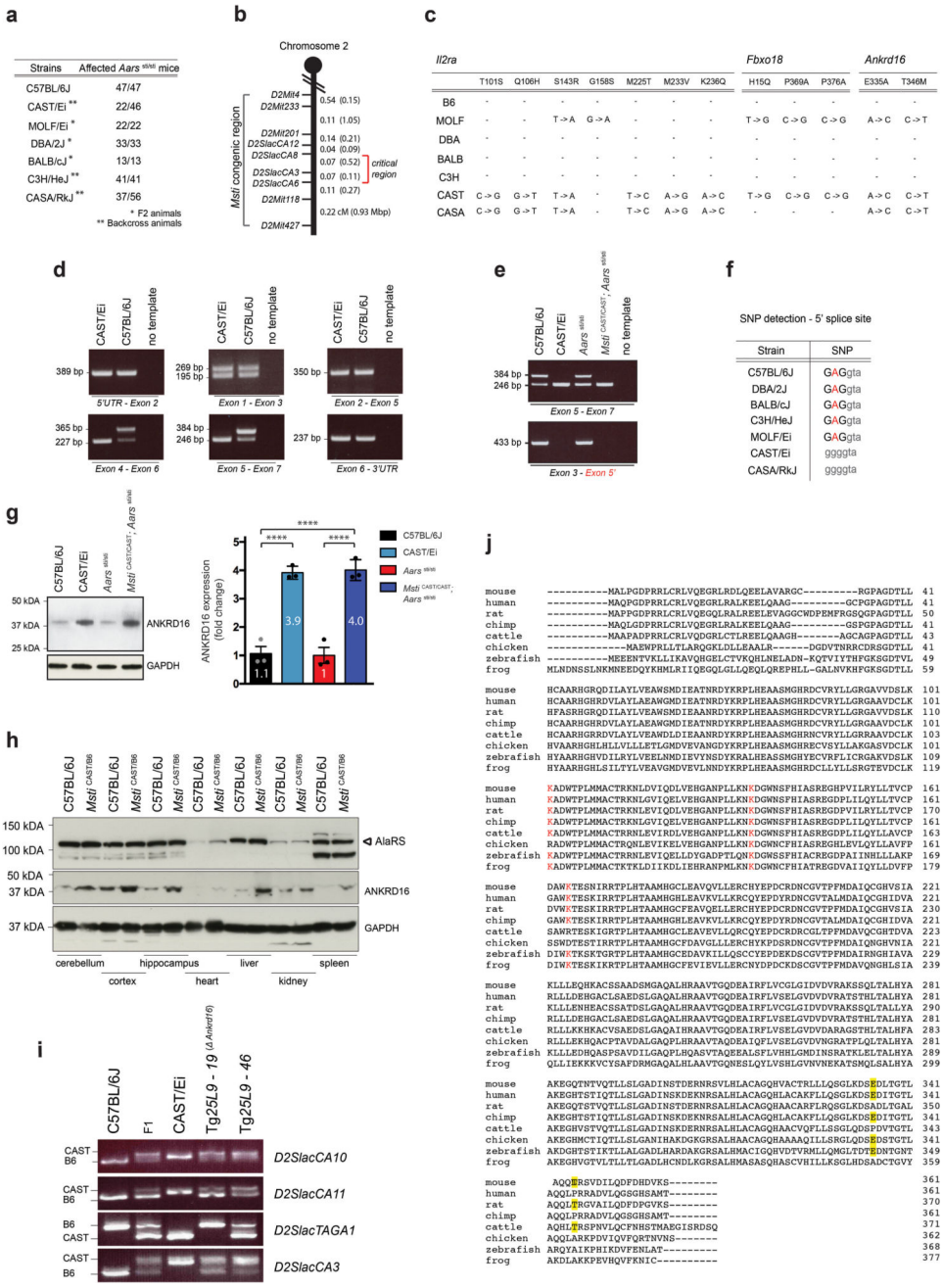

Extended Data Figure 1. Identification of *Ankrd16* as a genetic modifier of the B6J.*Aars*$^{sti/sti}$ mutation

a, 3- to 4-month-old *Aars*$^{sti/sti}$ mice from crosses to inbred strains. **b,** Location of *Msti* relative to microsatellite markers. Centimorgan (cM), megabase pairs (Mbp). **c,** Nonsynonymous SNPs in *Msti* candidate genes. The amino acids and position are shown at the top of the table with the B6 residue listed first. **d,** RT-PCR analysis of *Ankrd16* transcripts from cerebellar cDNA prepared from C57BL/6J and CAST/Ei mice. Note, the alternative *Ankrd16* transcript containing exon 5' (see Figure 2c) amplified by primers to

exon4/6 or exon 5/7 was present in cDNA from C57BL/6J but not CAST/Ei mice, whereas the alternative transcript detected by exon1/3 primers was present in cDNA from both strains. **e,** RT-PCR analysis of *Ankrd16* transcripts from cerebellar cDNA prepared from C57BL/6J, CAST/Ei, *Aars*$^{sti/sti}$, and *Msti*$^{CAST/CAST}$; *Aars*$^{sti/sti}$ mice. Note, the alternative *Ankrd16* transcript containing exon 5' (see Figure 2c) amplified by exon 5/7 or 3/5' primers was present in cDNA from C57BL/6J and *Aars*$^{sti/sti}$, but absent in the presence of CAST/Ei derived *Msti* (CAST/Ei and *Msti*$^{CAST/CAST}$; *Aars*$^{sti/sti}$ mice). **f,** Sequence of the SNP-containing region in intron 5 of *Ankrd16*. Capital letters indicate novel exon 5' and lower case letters indicate intron 5. The SNP in non-rescuing strains is shown in red. **g,** Western blotting analysis of ANKRD16 from cerebellar lysates. Note that the expression of ANKRD16 is reduced in C57BL/6J and *Aars*$^{sti/sti}$ mice relative to mice with CAST/Ei derived *Msti* (CAST/Ei and *Msti*$^{CAST/CAST}$; *Aars*$^{sti/sti}$ mice) (mean ± SD, n = 3, One-way ANOVA (Tukey correction), **** $p \leq 0.0001$). **h**, Protein levels of AlaRS and ANKRD16 were determined by western blotting using various mouse tissues from C57BL/6J and B6 congenic mice heterozygous for the *Msti* region (*Msti*$^{CAST/B6}$). GAPDH is included as a loading control. Note the increase in ANKRD16 levels in *Msti*$^{CAST/B6}$ tissues, whereas AlaRS levels do not change between genotypes. **i,** PCR results of genomic DNA from B6 transgenic mouse lines Tg25L9-19 and Tg25L9-46, which carry the CAST/Ei BAC. Polymorphic markers, which differentiate between C57BL/6J and CAST/Ei were used as shown. **j,** Amino acid sequence comparison of ANKRD16 from various species with the C57BL/6J strain shown. Non-synonymous SNPs distinguishing CAST/Ei and C57BL/6J are shown in yellow and serinylated lysines are shown in red.

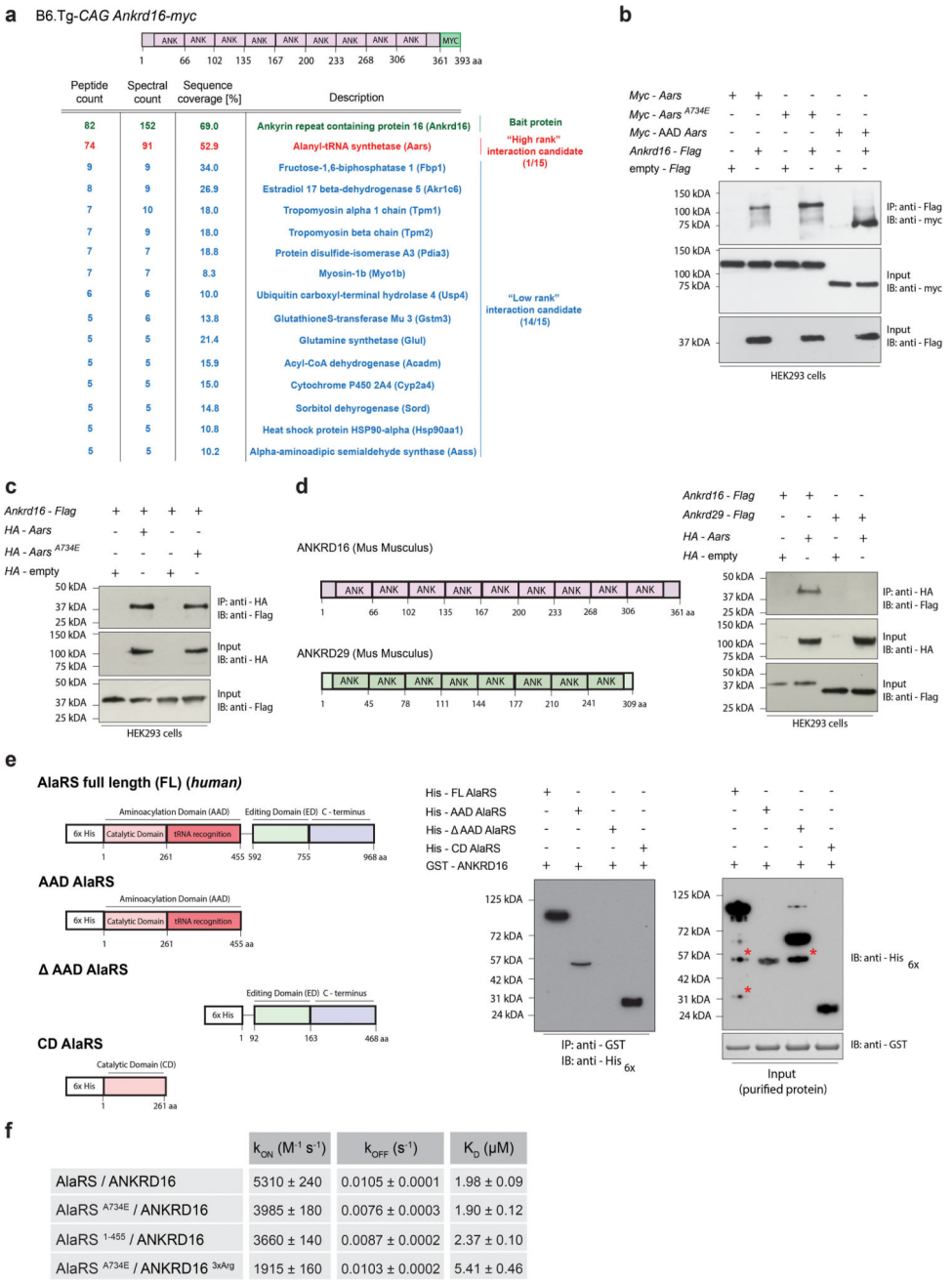

Extended Data Figure 2. Verification of interaction between ANKRD16 and AlaRS *in vitro*

a, Peptide/spectral counts of proteins co-immunoprecipitated (Co-IP) from transgenic *Ankrd16-myc* (see cartoon) but not detected in non-transgenic liver tissue. **b,** HEK293T cells were transiently co-transfected with myc-tagged constructs for mouse *Aars, Aars*^{A734E}, the *Aars* aminoacylation domain (AAD), and FLAG-tagged *Ankrd16*. Co-IP experiments were performed with ANKRD16-FLAG as the bait protein. **c,** Reciprocal Co-IP experiments were performed by transiently co-transfecting HEK293T cells with HA-tagged constructs for mouse *Aars* or *Aars*^{A734E} and the FLAG-tagged *Ankrd16*. HA-AlaRS proteins were used as bait for pull down. **d,** Domain structure of mouse ANKRD16 and ANKRD29. HEK293T

cells were transiently transfected with FLAG-tagged constructs for mouse *Ankrd16, Ankrd29,* and the HA-epitope tagged *Aars*. Co-IP experiments were performed with HA-AlaRS as bait protein. **e**, Various domain protein products of AlaRS (human) as indicated were bacterially expressed, purified, and incubated with GST-ANKRD16. GST-pull down products and input were immunoblotted with anti-His or -GST antibodies. Asterisks indicate protein degradation products. **f**, Binding dynamics were determined between mouse wild type or mutant AlaRS and mouse wild type or mutant ANKRD16 using SwitchSENSE (mean ± SD; n = 3).

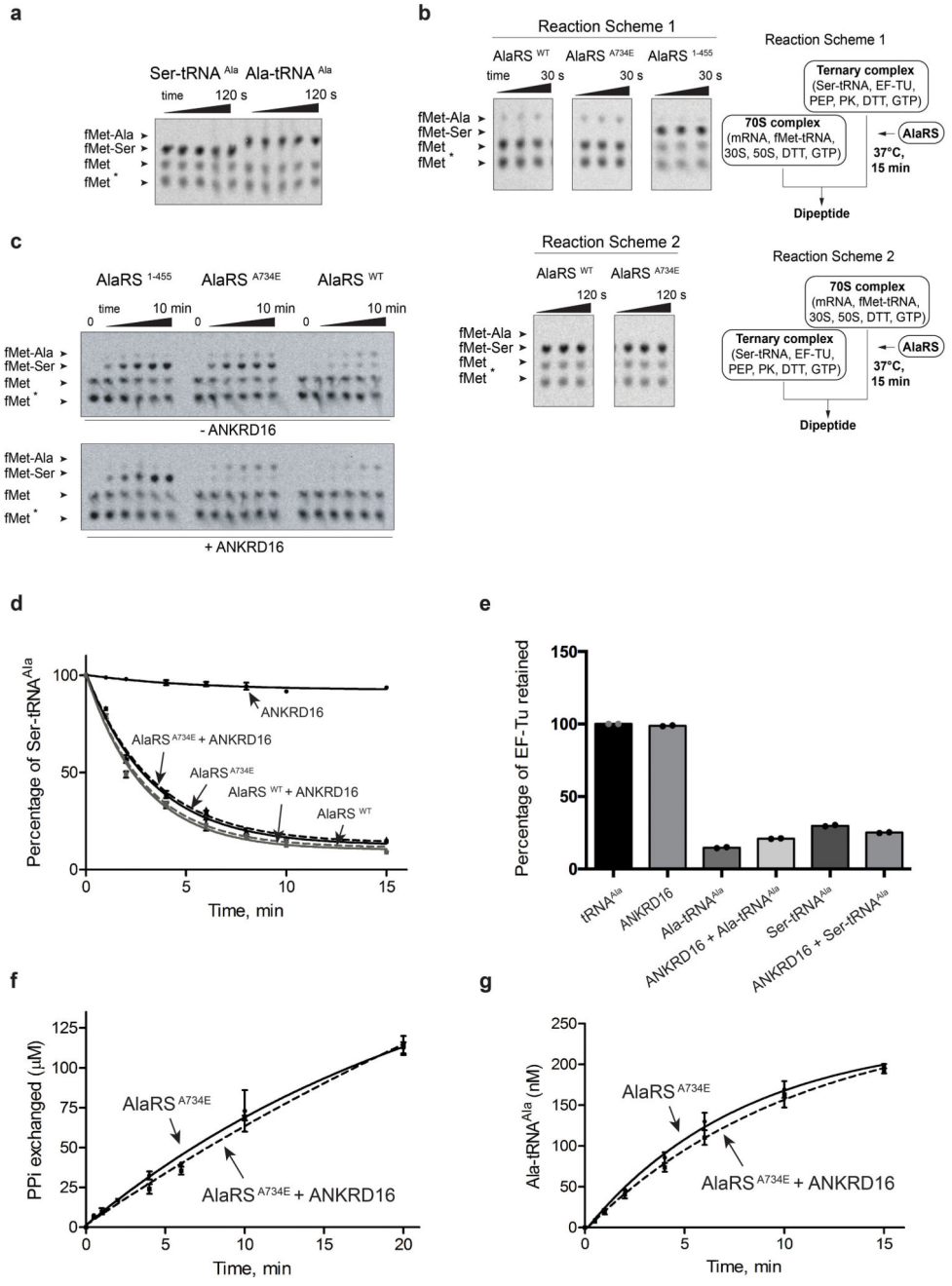

Extended Data Figure 3. Analysis of the effects of ANKRD16 on steps of translation

a, Preassembled ternary complex containing either Ser-tRNA^{Ala} or Ala-tRNA^{Ala} was mixed with 70S initiation complex (IC) programmed with codon GCU in the A site, aliquots were transferred at various times to quench solution (0.5 M KOH), and products were resolved by eTLC. **b,** Incubation of full-length AlaRS with preassembled EF-Tu•GTP•Ser-tRNA^{Ala} prevents fMet-Ser formation. EF-Tu•GTP•Ser-tRNA^{Ala} ternary complex and 70S IC were each preassembled. In reaction scheme 1, AlaRS was incubated with EF-Tu•GTP•Ser-tRNA^{Ala} for 15 min, 70S IC was added, and aliquots were removed at various times for eTLC analysis. In contrast (reaction scheme 2), AlaRS was incubated with the 70S IC for 15 min, followed by addition of EF-Tu•GTP•Ser-tRNA^{Ala}, and aliquots were removed at various times for eTLC analysis. **c**, Deacylated tRNA^{Ala} was mixed with AlaRS, serine, ATP, and all other components to form ternary complex, aliquots were transferred at various time points to the 70S IC, and dipeptide products were resolved by eTLC. t = 0 (control reactions in the absence of AlaRS); * (oxidized fMet). Note, without alanine supplementation (b and c), trace amounts of fMet-Ala are detected, likely due to AlaRS-bound alanyl-AMP during protein purification. **d**, Deacylation of [^{3}H]Ser-tRNA^{Ala} by mouse wild-type AlaRS or AlaRS^{A734E} in the presence or absence of ANKRD16 (mean ± SD, n = 2, One Phase Decay model [$R^2_{AlaRS^{WT}}$ = 0.9892; $R^2_{AlaRS^{A734E}}$ = 0.991; $R^2_{AlaRS^{WT}/ANKRD16}$ = 0.9872; $R^2_{AlaRS^{A734E}/ANKRD16}$ = 0.9902; $R^2_{ANKRD16^{3xArg}}$ = 0.7992]). **e**, Percentage of EF-Tu retained on filter membrane upon addition of various components as indicated (mean ± SD; n = 2). **f**, ATP-pyrophosphate exchange by mouse AlaRS^{A734E} in the presence or absence of ANKRD16 (mean ± SD, n = 2, Michaelis-Menten model [$R^2_{AlaRS^{A734E}}$ = 0.9763; $R^2_{AlaRS^{A734E}/ANKRD16}$ = 0.9874]). **g**, Aminoacylation of tRNA^{Ala} with alanine by mouse AlaRS^{A734E} in the presence or absence of ANKRD16 (mean ± SD, n = 2, Michaelis-Menten model [$R^2_{AlaRS^{A734E}}$ = 0.9879; $R^2_{AlaRS^{A734E}/ANKRD16}$ = 0.9846]).

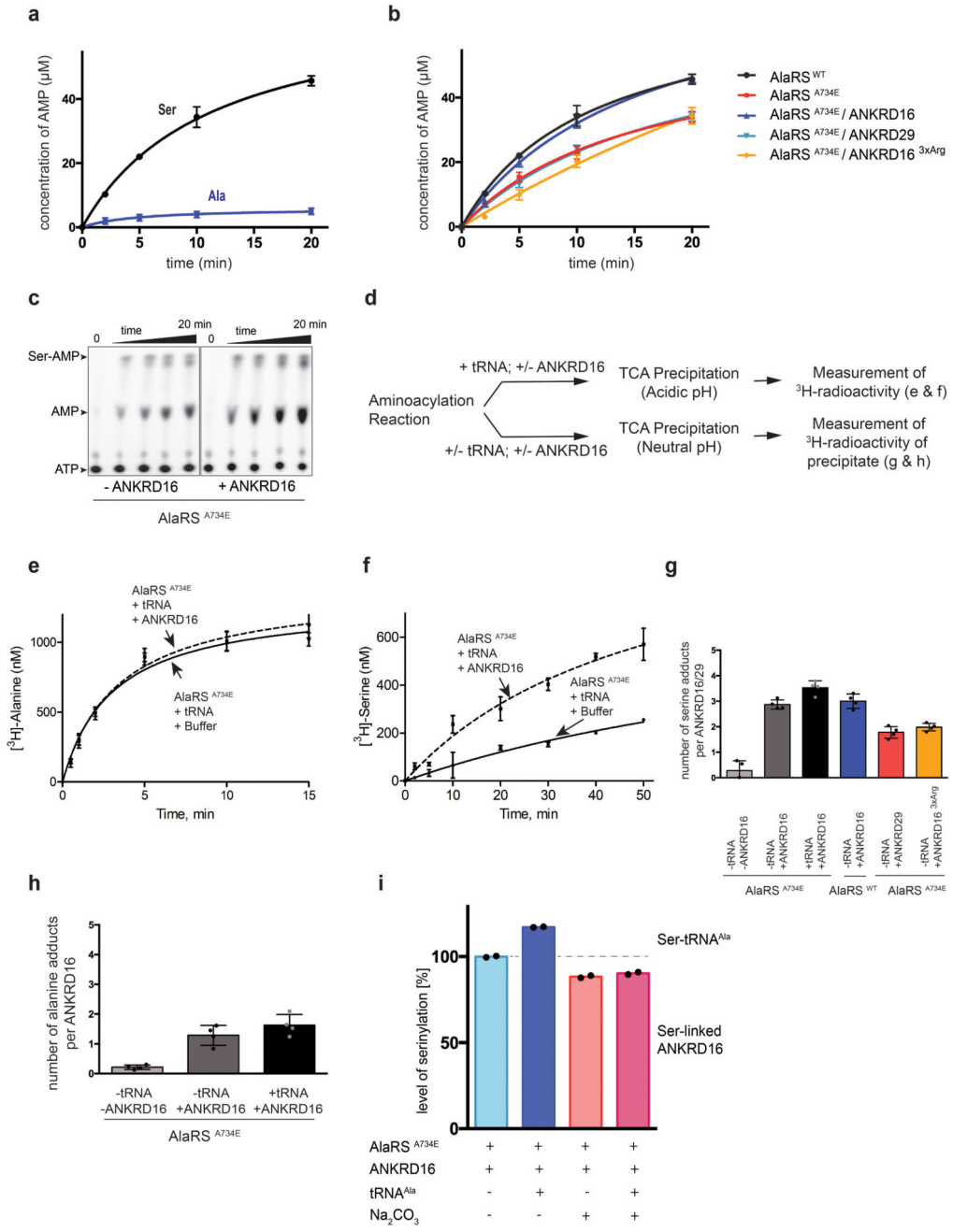

Extended Data Figure 4. Analysis of serinylation of ANKRD16

a, tRNA-independent ATPase activity of mouse wild type AlaRS for serine or alanine (mean ± SD, n = 3, Michaelis-Menten model [R^2_{Ser} = 0.9926; R^2_{Ala} = 0.8430]). **b,** tRNA-independent ATPase activity of mouse AlaRS^{WT} or AlaRS^{A734E} for serine in the presence of ANKRD16, ANKRD29, or ANKRD16^{3xArg} (mean ± SD, Michaelis-Menten model [$R^2_{AlaRS^{WT}}$ = 0.9926, $R^2_{AlaRS^{A734E}}$ = 0.9899, $R^2_{AlaRS^{A734E}/ANKRD16}$ = 0.9918, $R^2_{AlaRS^{A734E}/ANKRD29}$ = 0.9939, $R^2_{AlaRS^{A734E}/ANKRD16^{3xArg}}$ = 0.9841], [AlaRS^{WT}, AlaRS^{A734E}, AlaRS^{A734E}/ANKRD29, n = 3], [AlaRS^{A734E}/ANKRD16, AlaRS^{A734E}/ANKRD16^{3xArg}, n = 4]). **c,** TLC analysis of ATPase activity of AlaRS^{A734E} against serine

in the absence and presence of ANKRD16. **d,** Experimental scheme showing how data were generated for panels **e, f, g,** and **h. e,** Acylation reactions with radioactive alanine were performed as above to determine alanine transfer (mean ± SD, n = 2, Michaelis-Menten model [$R^2_{AlaRS^{A734E}/tRNA/ANKRD16}$ = 0.9611, $R^2_{AlaRS^{A734E}/tRNA/buffer}$ = 0.9641]). **f**, Misacylation of $tRNA^{Ala}$ with radioactive serine by mouse $AlaRS^{A734E}$ in the presence or absence (buffer) of ANKRD16. After misacylation, reactions were subjected to TCA precipitation of RNA (Ser-$tRNA^{Ala}$) and protein under acidic conditions to maintain Ser-tRNA (mean ± SD, n = 2, Michaelis-Menten model [$R^2_{AlaRS^{A734E}/tRNA/ANKRD16}$ = 0.9577, $R^2_{AlaRS^{A734E}/tRNA/buffer}$ = 0.7841]). **g,** Misacylation reactions using radioactive serine and mouse $AlaRS^{WT}$ or $AlaRS^{A734E}$ were performed in the presence or absence of ANKRD16, ANKRD29, $ANKRD16^{3xArg}$, or $tRNA^{Ala}$. After TCA precipitation under neutral pH conditions, serine was measured (mean ± SD, n = 4). Note, the higher level of TCA-precipitated serine on tRNA or protein in the presence of ANKRD16. **h,** Acylation reactions using radioactive alanine and mouse $AlaRS^{A734E}$ were performed in the presence or absence of ANKRD16 or $tRNA^{Ala}$. After TCA precipitation under neutral pH conditions, alanine was measured (mean ± SD, n = 4). **i,** Misacylation reactions using radioactive serine and mouse $AlaRS^{A734E}$ were performed in the presence of ANKRD16 either with or without $tRNA^{Ala}$. Reactions were treated with or without Na_2CO_3 (final concentration of 0.15 M [alkaline pH]) for 30 minutes, followed by TCA precipitation. Precipitated [^{3}H]-serine-links were measured and plotted as relative level of serinylation (mean, n = 2).

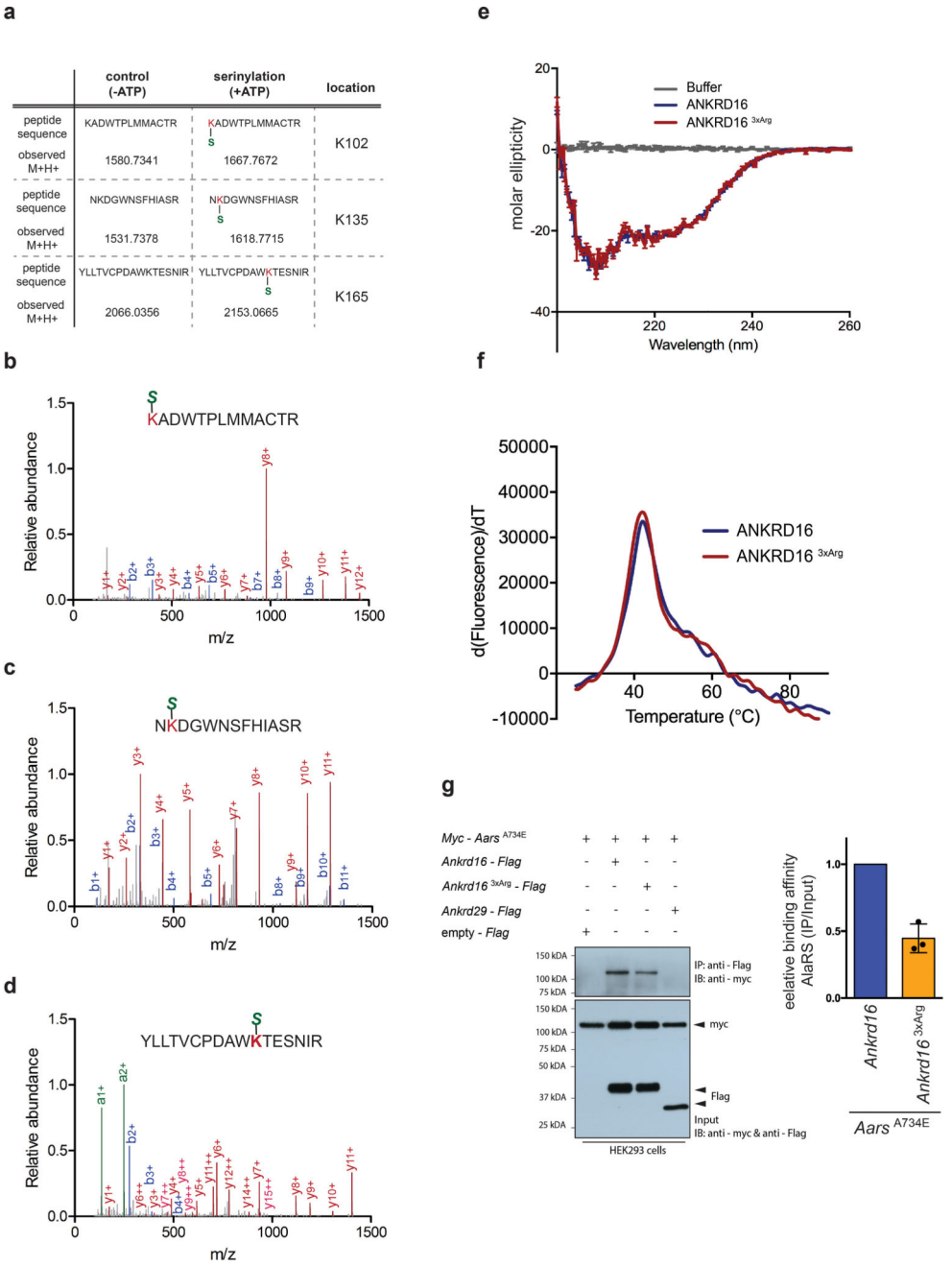

Extended Data Figure 5. Analysis of serinylation of ANKRD16 by mass spectrometry

a, MS/MS spectrum of peptides from ANKRD16. Incorporation of serine onto ANKRD16 was observed when serine was misactivated by mouse AlaRS^{A734E} (+ATP). Misactivation was not observed in the absence of ATP. MS/MS spectrum of peptides from ANKRD16 with serine linked to positions K102 (**b**), K135 (**c**) and K165 (**d**). a ions [a], b ions [b] and y ions [y] are annotated in green, red, and purple, respectively. The triply charged precursor had a mass of 2153.065 Dalton and included carbamidomethyl cysteine. **e,** Secondary structure analysis of mouse ANKRD16 and ANKRD16^{3xArg}. Far-UV circular dichroism (CD) spectra of wild type ANKRD16 (blue) and ANKRD16^{3xArg} (red) show highly similar CD spectra

(mean ± SD, n = 4). **f,** Thermal shift analysis of mouse ANKRD16 (blue) and ANKRD16^{3xArg} (red) show highly similar thermal stability. **g,** HEK293T cells were transiently co-transfected with myc-tagged constructs for mouse *Aars*^{A734E} and FLAG-tagged *Ankrd16, Ankrd16*^{3xArg}, or *Ankrd29.* Co-IP experiments were performed with FLAG-tagged proteins as the bait protein. Binding affinity was determined by normalizing immunoprecipitation (IP) signal of AlaRS^{A734E} to the input signal, in which the interaction of AlaRS^{A734E}/ANKRD16 was arbitrarily defined as 1 to determine relative binding affinity of AlaRS^{A734E}/ANKRD16^{3xArg} (mean ± SD, n = 3).

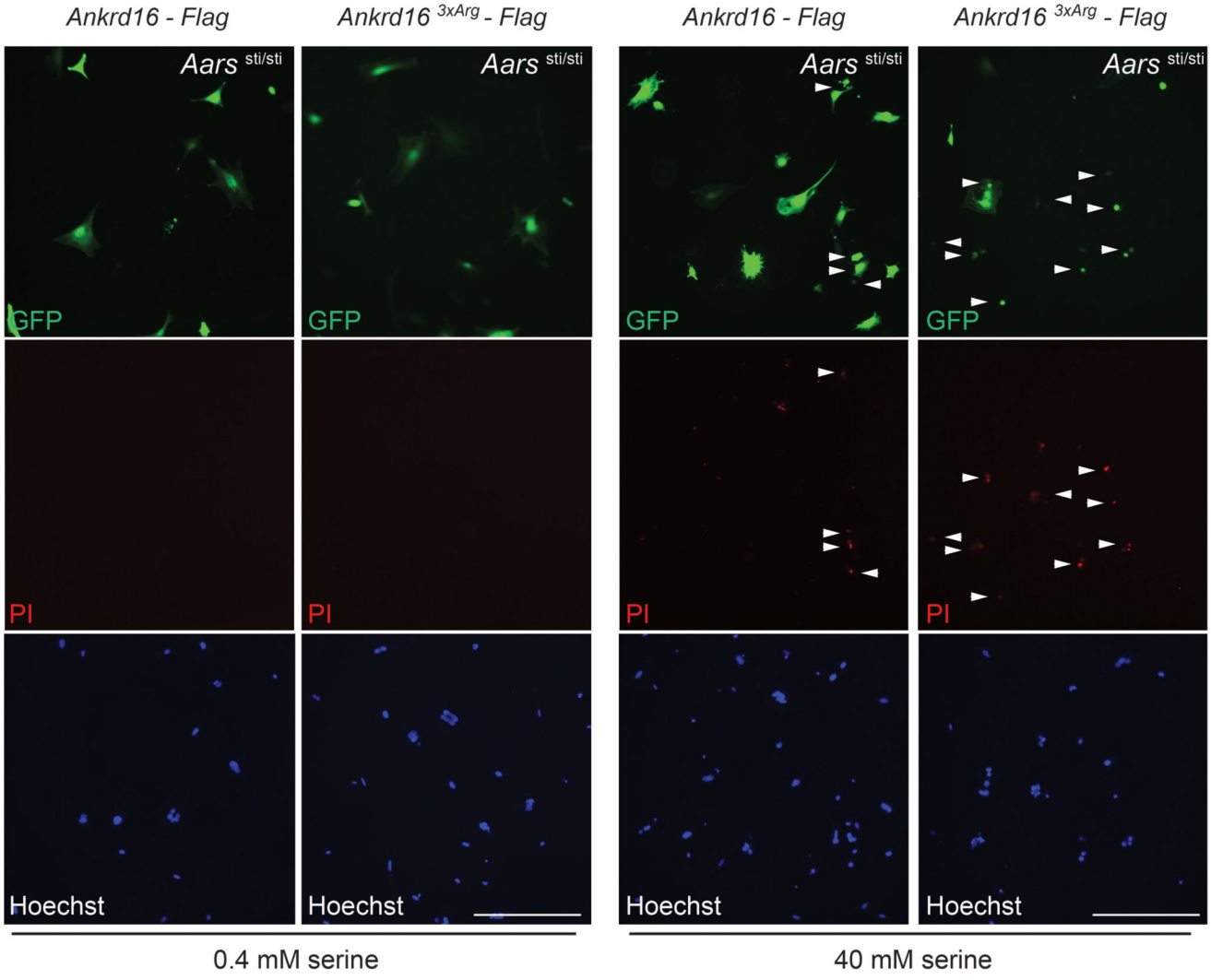

Extended Data Figure 6. Serine-induced cell death in *Aars*$^{sti/sti}$ fibroblasts

B6.*Aars*$^{sti/sti}$ embryonic fibroblasts were co-transfected with hrGFP (humanized recombinant GFP, green) and either *Ankrd16-Flag or Ankrd16*^{3xArg}*-Flag* (n = 4). 12-hours post-transfection, serine was added and cells were cultured for 24 hours prior to staining with propidium iodide (PI) (red) and Hoechst (blue) to determine cell death. Arrowheads represent PI-positive GFP^{+} cells. Scale bars: 100 μm.

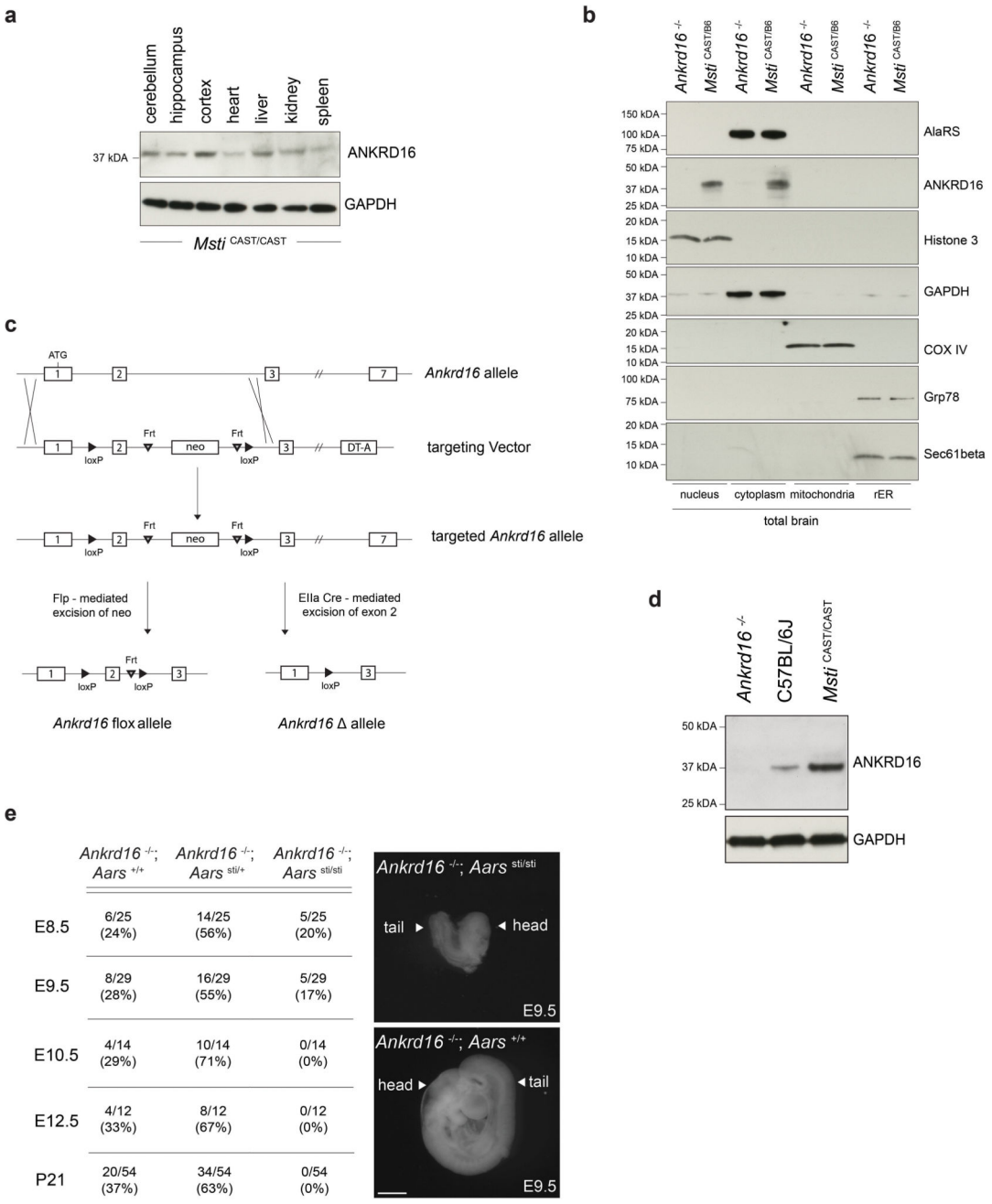

Extended Data Figure 7. Analysis of ubiquitous deletion of ANKRD16

a, Protein levels of ANKRD16 were determined by western blotting of tissues from B6 mice homozygous for the *Msti* region (*Msti*$^{CAST/CAST}$). **b,** Subcellular analysis of ANKRD16 and AlaRS via cell fractionation of brains from B6.*Msti*$^{CAST/B6}$ and *Ankrd16*$^{-/-}$ mice. Cellular fractions were confirmed using antibodies for histone 3 (nuclear marker), GAPDH (cytosolic marker), COX IV (mitochondrial marker), GRP78 (ER marker), and Sec61 beta (rough ER marker). **c,** To generate a ubiquitous or conditional loss-of-function allele, *lox*P sites that flank exon 2 of *Ankrd16* were inserted by homologous recombination. Removal of exon 2 results in a frame shift and premature stop codon in exon 3. *Ankrd16* was ubiquitously

deleted by EIIa Cre-mediated removal of exon 2 and the neo cassette. Flp-mediated excision of the neomycin cassette was utilized to generate a conditional loss-of-function *Ankrd16* allele. **d,** Loss of ANKRD16 was verified by western blotting. Protein extracts from *Ankrd16*$^{-/-}$, *Msti*$^{CAST/CAST}$ and C57BL/6J mice were used for comparison purposes and GAPDH was used as a loading control. **e,** The number of embryos or mice of various genotypes from intercrosses of *Aars*$^{sti/+}$; *Ankrd16*$^{-/-}$ mice over the total number observed. Representative images of E9.5 embryos. Note, *Aars*$^{sti/sti}$; *Ankrd16*$^{-/-}$ embryos are smaller and have failed to turn. Abbreviations: embryonic day (E), postnatal day (P). Scale bars: 500 μm.

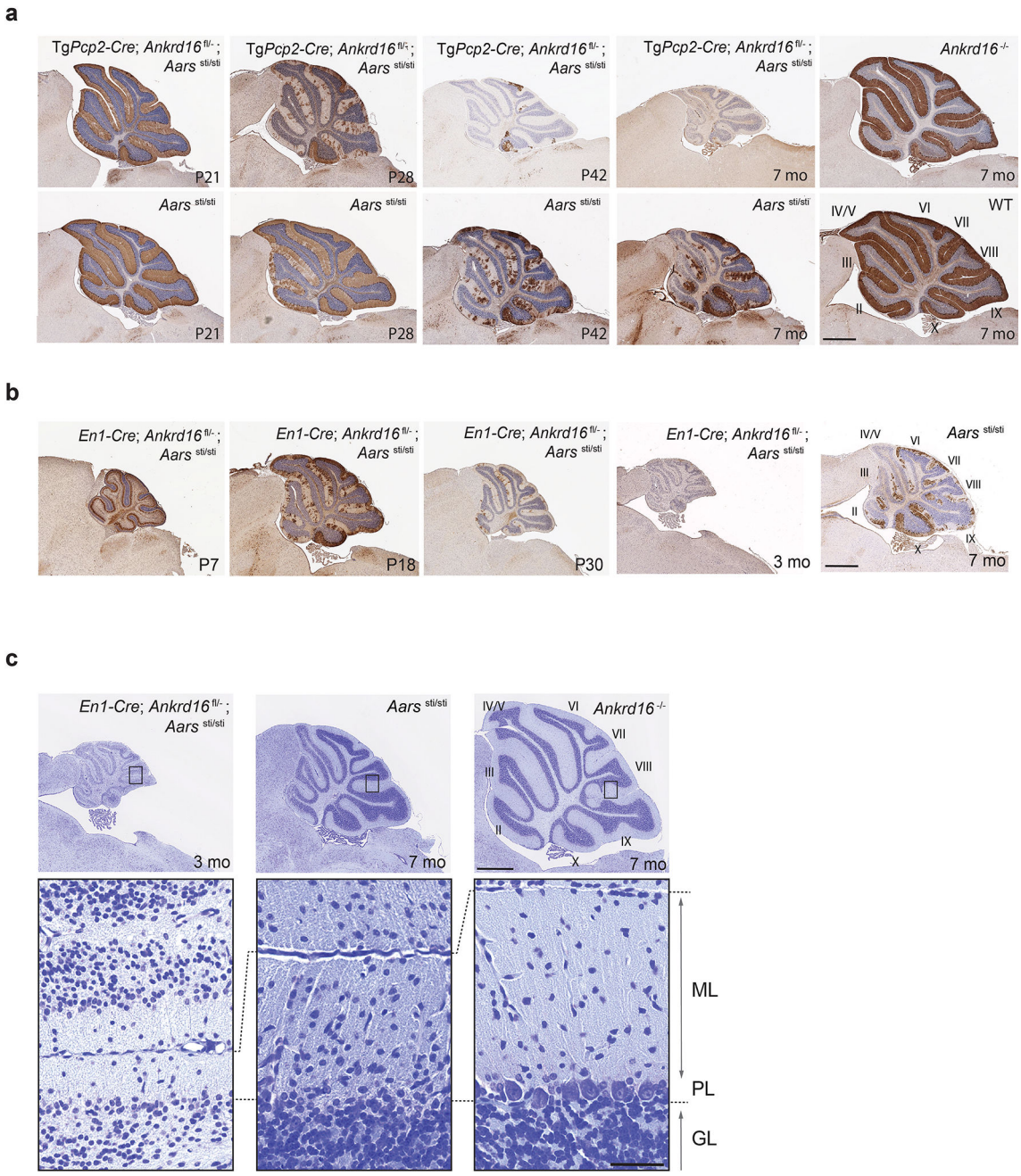

Extended Data Figure 8. Conditional deletion of *Ankrd16* accelerates Purkinje cell loss and causes widespread neurodegeneration in the B6.*Aars*$^{sti/sti}$ cerebellum

a and **b,** Calbindin D-28 immunohistochemistry of sagittal cerebellar sections. c, Cresyl violet-stained sagittal cerebellar sections. Note, the presence of interneurons in the ML of B6.*Aars*$^{sti/sti}$ cerebellum despite the thinning of the ML as a consequence of Purkinje cell degeneration. In contrast, loss of *Ankrd16* in the B6.*Aars*$^{sti/sti}$ cerebellum results in degeneration of ML interneurons. Scale bars: 500 μm (**a, b, c**), 50 μm (**c**, higher magnification). Abbreviations: postnatal day (P), molecular layer (ML), Purkinje cell layer (PL), granule cell layer (GL).

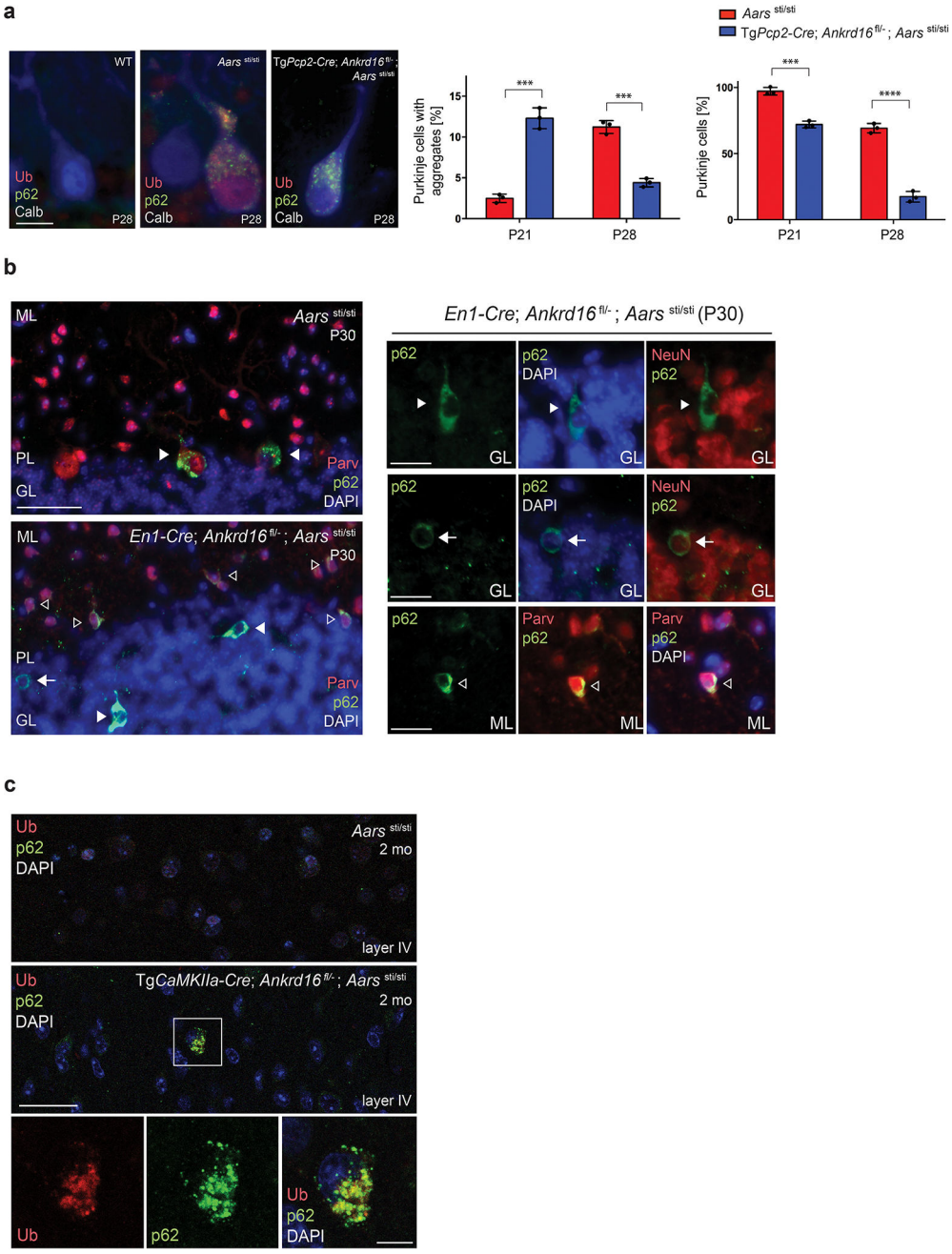

Extended Data Figure 9. Conditional deletion of *Ankrd16* accelerates formation of protein aggregates in B6.*Aars*$^{sti/sti}$ mice

a, Ubiquitin (red), p62 (green), and Calbindin D-28 (blue) immunofluorescence on sagittal cerebellar sections. The percentage of aggregate-positive Purkinje cells and Purkinje cells are shown (mean ± SD, n = 3, Multiple t-tests (Holm-Sidak method), *** p = 0.0002466 (Purkinje cells with aggregates, P21), p = 0.0002336 (Purkinje cells with aggregates, P28), p = 0.0003214 (percent of Purkinje cells, P21), **** p = 7.701787×10^{-5} (percent of Purkinje cells, P28)). Note, the percent of Purkinje cells is relative to control C57BL/6J mice. **b,** Cell type-specific markers (red), and p62 (green) immunofluorescence on sagittal cerebellar sections. Parvalbumin (Parv) was utilized to identify Purkinje cells and interneurons (stellate

and basket cells) in the ML. NeuN was utilized to distinguish between granule and Golgi cells in the GL. (En1-Cre; *Ankrd16*$^{fl/-}$; *Aars*$^{sti/sti}$: Golgi cell [closed arrow head, p62^{+}/NeuN^{-}]; granule cell [arrow, p62^{+}/NeuN^{+}]; basket/stellate cell [open arrow head, p62^{+}/Parv^{+}]). **c,** Ubiquitin (red) and p62 (green) immunofluorescence on sagittal sections of the cortex (layer IV). Scale bars: 10 μm (**a**), 50 μm (**b** and **c**, low magnification) and 10 μm (**b** and **c**, higher magnification). Abbreviations: postnatal day (P), molecular layer (ML), Purkinje cell layer (PL), granule cell layer (GL).

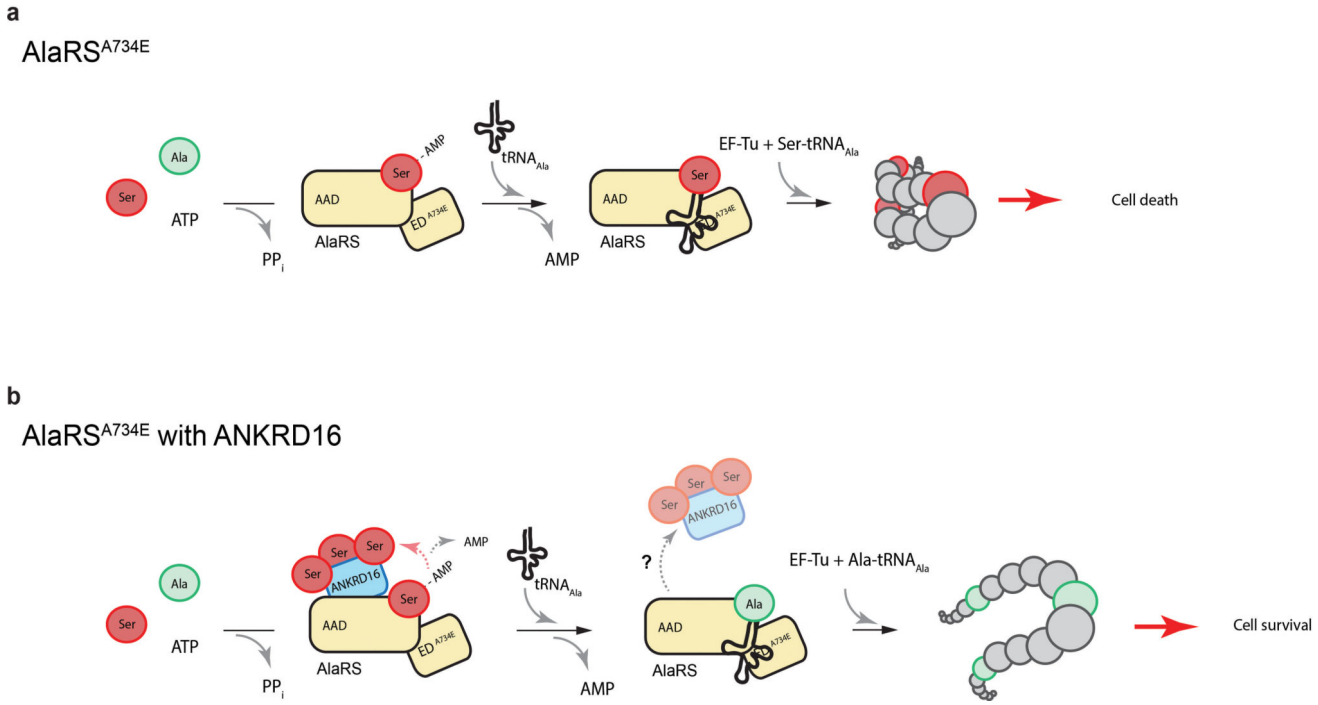

Extended Data Figure 10. Model for the role of ANKRD16 in translational fidelity

a, A point mutation in the editing domain of AlaRS (A734E) results in editing defects, as indicated by deficits in tRNA-independent ATPase activity, which in turn leads to increased levels of incorrectly aminoacylated Ser-tRNA^{Ala}, misincorporation of serine during translation, protein aggregation, and cell death. **b,** Interaction of ANKRD16 with the aminoacylation domain of editing-deficient AlaRS^{A734E} stimulates tRNA-independent editing and misactivated serines are transferred onto ANKRD16. Mitigation of serine misactivation prevents *sti*-mediated mistranslation, and thereby prevents protein aggregation and cell death.

Supplementary Material

Refer to Web version on PubMed Central for supplementary material.

Acknowledgments

We thank K. Brown, J. Cook, T. Jucius, and A. Kano for technical assistance and the microinjection core at The Jackson Laboratory for transgenic mouse production. This work was supported by National Institutes of Health R01NS42613 to S.L.A., R01GM072528 to K.F., R01CA92577 and a Fellowship from the National Foundation for Cancer Research to P.S. S.L.A. is an investigator of the Howard Hughes Medical Institute.

References

1. Guo M, Chong YE, Shapiro R, Beebe K, Yang XL, Schimmel P. Paradox of mistranslation of serine for alanine caused by AlaRS recognition dilemma. Nature. 2009; 462:808–812. [PubMed: 20010690]
2. Schimmel P. Mistranslation and its control by tRNA synthetases. Philos. Trans. R. Soc. B Biol. Sci. 2011; 366:2965–2971.
3. Ling J, Reynolds N, Ibba M. Aminoacyl-tRNA synthesis and translational quality control. Annu. Rev. Microbiol. 2009; 63:61–78. [PubMed: 19379069]
4. Martinis SA, Boniecki MT. The balance between pre- and post-transfer editing in tRNA synthetases. FEBS Lett. 2010; 584:455–459. [PubMed: 19941860]
5. Dulic M, Cvetesic N, Perona JJ, Gruic-Sovulj I. Partitioning of tRNA-dependent editing between pre- and post-transfer pathways in class I aminoacyl-tRNA synthetases. J. Biol. Chem. 2010; 285:23799–23809. [PubMed: 20498377]
6. Schimmel P. Development of tRNA synthetases and connection to genetic code and disease. Protein Sci. 2008; 17:1643–1652. [PubMed: 18765819]
7. Beebe K, Pouplana LRDe, Schimmel P. Elucidation of tRNA-dependent editing by a class II tRNA synthetase and significance for cell viability. EMBO. 2003; 22
8. Nangle LA, Motta CM, Schimmel P. Global effects of mistranslation from an editing defect in mammalian cells. Chem. Biol. 2006; 13:1091–1100. [PubMed: 17052613]
9. Lee JW, Beebe K, Nangle LA, Jang J, Longo-Guess CM, Cook SA, Davisson MT, Sundberg JP, Schimmel P, Ackerman SA. Editing-defective tRNA synthetase causes protein misfolding and neurodegeneration. Nature. 2006; 443:50–55. [PubMed: 16906134]
10. Lu J, Bergert M, Walther A, Suter B. Double-sieving-defective aminoacyl-tRNA synthetase causes protein mistranslation and affects cellular physiology and development. Nat. Commun. 2014; 5:5650. [PubMed: 25427601]
11. Liu Y, Satz JS, Vo MN, Nangle LA, Schimmel P, Ackerman SL. Deficiencies in tRNA synthetase editing activity cause cardioproteinopathy. Proc. Natl. Acad. Sci. 2014; 111:17570–17575. [PubMed: 25422440]
12. Calendar R, Berg P. D-tyrosyl RNA: formation, hydrolysis and utilization for protein synthesis. J. Mol. Biol. 1967; 26:39–54. [PubMed: 4292198]
13. Pawar KI, Suma K, Seenivasan A, Kuncha SK. Role of D-aminoacyl-tRNA deacylase beyond chiral proofreading as a cellular defense against glycine mischarging by AlaRS. Elife. 2017
14. Calendar R. D-tyrosyl-tRNA deacylase: a new function. Trends Biochem. Sci. 2017; 42:684–686. [PubMed: 28764927]
15. Hitoshi N, Ken-ichi Y, Jun-ichi M. Efficient selection for high-expression transfectants with a novel eukaryotic vector. Gene. 1991; 108:193–199. [PubMed: 1660837]
16. Okabe M, Ikawa M, Kominami K, Nakanishi T, Nishimune Y. 'Green mice' as a source of ubiquitous green cells. FEBS Lett. 1997; 407:313–319. [PubMed: 9175875]
17. Tsui WC, Fersht AR. Probing the principles of amino acid selection using the alanyl-tRNA synthetase from Escherichia coli. Nucleic Acids Res. 1981; 9:4627–4637. [PubMed: 6117825]
18. Yanagisawa T, Sumida T, Ishii R, Takemoto C, Yokoyama S. A paralog of lysyl-tRNA synthetase aminoacylates a conserved lysine residue in translation elongation factor P. Nat. Struct. Mol. Biol. 2010; 17:1136–1143. [PubMed: 20729861]
19. He X, et al. Sensing and transmitting intracellular amino acid signals through reversible lysine aminoacylations. Cell Metab. 2018; 27:151–166. [PubMed: 29198988]
20. Jakubowski H. Protein homocysteinylation: possible mechanism underlying pathological consequences of elevated homocysteine levels. FASEB J. 1999; 13:2277–2283. [PubMed: 10593875]
21. Jakubowski H. Quality control in tRNA charging - editing of homocysteine. Acta Biochim. Pol. 2011; 58:149–163. [PubMed: 21643559]

22. Kimmel RA, Turnbull DH, Blanquet V, Wurst W, Loomis CA, Joyner AL. Two lineage boundaries coordinate vertebrate apical ectodermal ridge formation. Genes Dev. 2000; 14:1377–1389. [PubMed: 10837030]
23. Beebe K, Mock M, Merriman E, Schimmel P. Distinct domains of tRNA synthetase recognize the same base pair. Nature. 2008; 451:90–93. [PubMed: 18172502]
24. Chong YE, Yang XL, Schimmel P. Natural homolog of tRNA synthetase editing domain rescues conditional lethality caused by mistranslation. J. Biol. Chem. 2008; 283:30073–30078. [PubMed: 18723508]
25. Fersht AR. Editing Mechanisms in Protein-Synthesis - Rejection of valine by isoleucyl-transfer-RNA Synthetase. Biochemistry. 1977; 16:1025–1030. [PubMed: 321008]
26. Jakubowski H, Goldman E. Editing of errors in selection of amino acids for protein synthesis. Microbiol. Rev. 1992; 56:412–429. [PubMed: 1406490]
27. Ibba M, Söll D. Quality control mechanisms during translation. Science. 1999; 286:1893–1897. [PubMed: 10583945]
28. Van Ham TJ, Breitling R, Swertz MA, Nollen EAA. Neurodegenerative diseases: Lessons from genome-wide screens in small model organisms. EMBO Mol. Med. 2009; 1:360–370. [PubMed: 20049741]
29. Chen X, Burgoyne RD. Identification of common genetic modifiers of neurodegenerative diseases from an integrative analysis of diverse genetic screens in model organisms. BMC Genomics. 2012; 13:71. [PubMed: 22333271]
30. Lenz S, Karsten P, Schulz JB, Voigt A. Drosophila as a screening tool to study human neurodegenerative diseases. J. Neurochem. 2013; 127:453–460. [PubMed: 24028575]

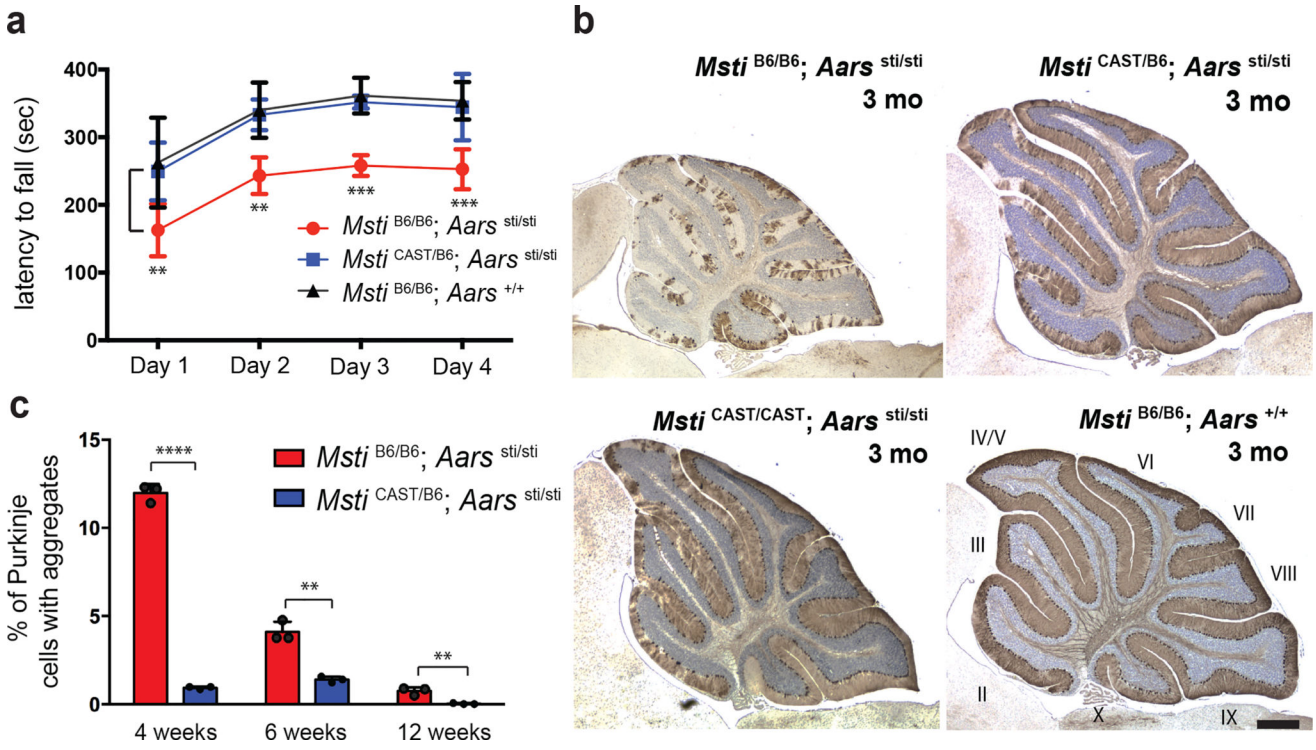

Figure 1. *Modifier of sticky (Msti)* suppresses *Aars*^{sti}-mediated neurodegeneration

a, Rotorod analysis of 3-month-old mice (mean ± SD, n = 15 or 16 mice/genotype, Two-way ANOVA (Tukey correction), ** $p \leq 0.01$, *** $p \leq 0.001$). **b,** Calbindin D-28 immunohistochemistry. Sections were counterstained with hematoxylin. **c,** Aggregate-positive cells (mean ± SD, n = 3, Multiple t-tests (Holm-Sidak method), ** p = 0.00148 (6 weeks), p = 0.00498 (12 weeks), **** $p = 2.819\times10^{-6}$). Scale bars: 500 μm.

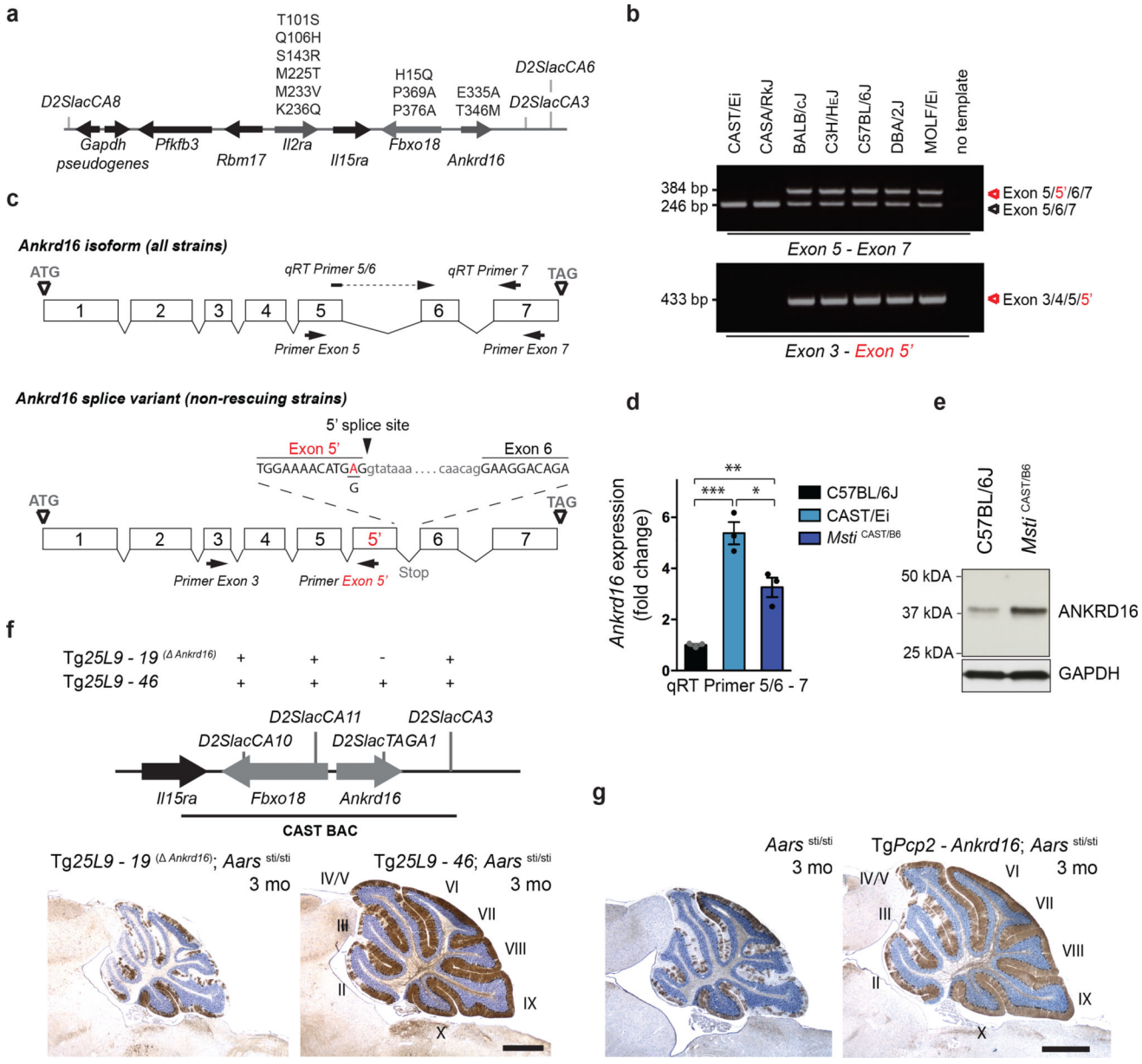

Figure 2. *Ankrd16* is the modifier of *Aars*$^{sti/sti}$

a, Amino acid polymorphisms between C57BL/6J and CAST/Ei in *Msti* region. **b,** Alternative splicing of *Ankrd16* in the cerebellum. **c,** An intronic SNP (red) introduces a cryptic exon (exon 5') in *Ankrd6* in non-*Msti* containing strains. **d,** Expression of correctly spliced *Ankrd16* in the cerebellum (mean ± SEM, n = 3, One-way ANOVA (Tukey correction), * $p \leq 0.05$, ** $p \leq 0.01$, *** $p \leq 0.001$). **e,** Western blot analysis using cerebellar extracts. **f** and **g,** Calbindin D-28 immunohistochemistry. Scale bars: 500 μm.

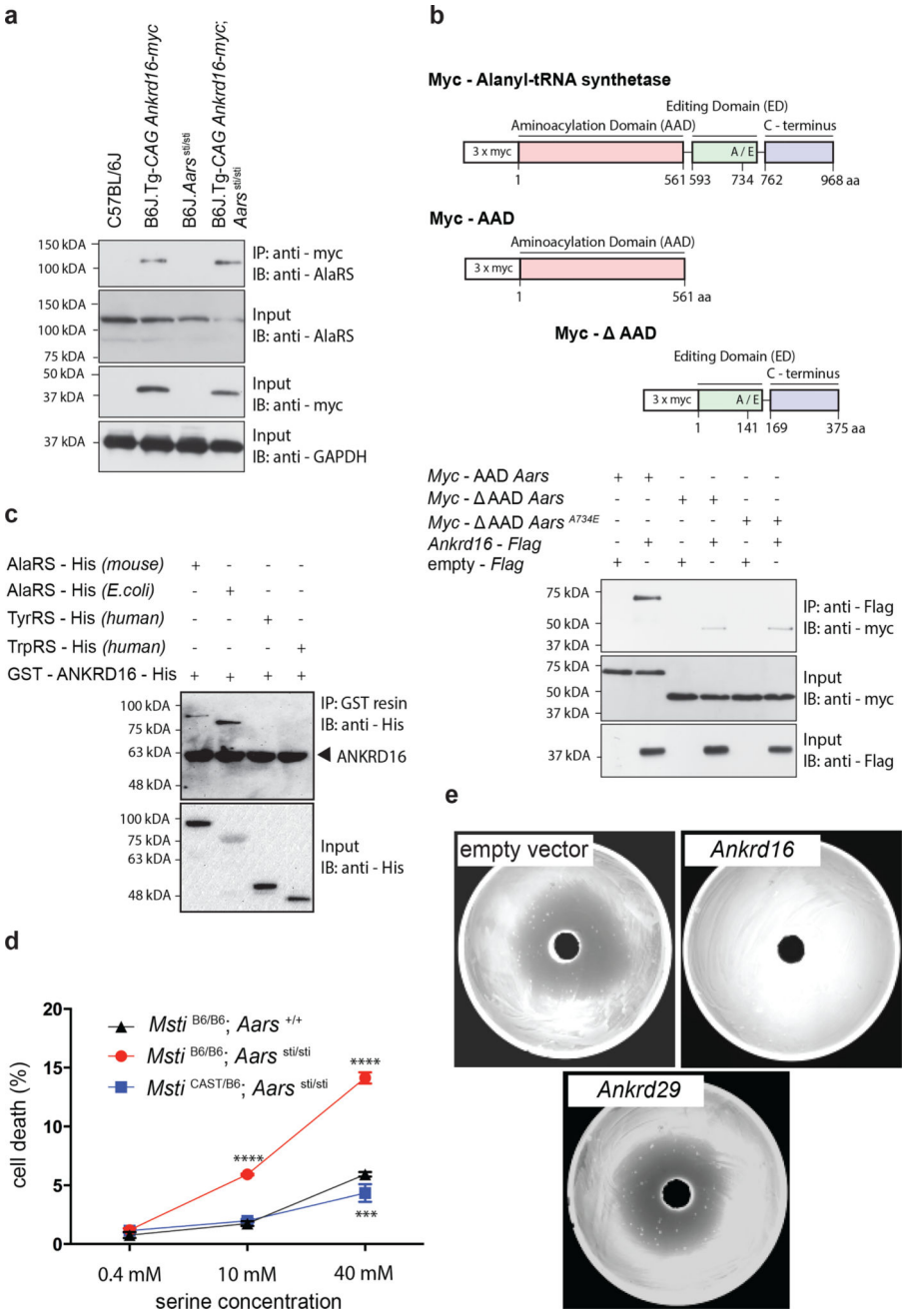

Figure 3. ANKRD16 interacts with AlaRS and prevents serine-mediated cell death

a, AlaRS/ANKRD16 interaction in the brain. **b,** Co-IP experiments in HEK293T cells using mouse myc-AlaRS domain constructs. **c,** Pull down of purified AlaRS, TyrRS, or TrpRS with ANKRD16. **d,** Cell death of embryonic fibroblasts (mean ± SD, n = 3, Two-way ANOVA (Tukey correction), *** $p \leq 0.001$; **** $p \leq 0.0001$). **e,** *Aars*$^{C666A/Q584H}$ *E. coli* expressing mouse *Ankrd16* or *Ankrd29*.

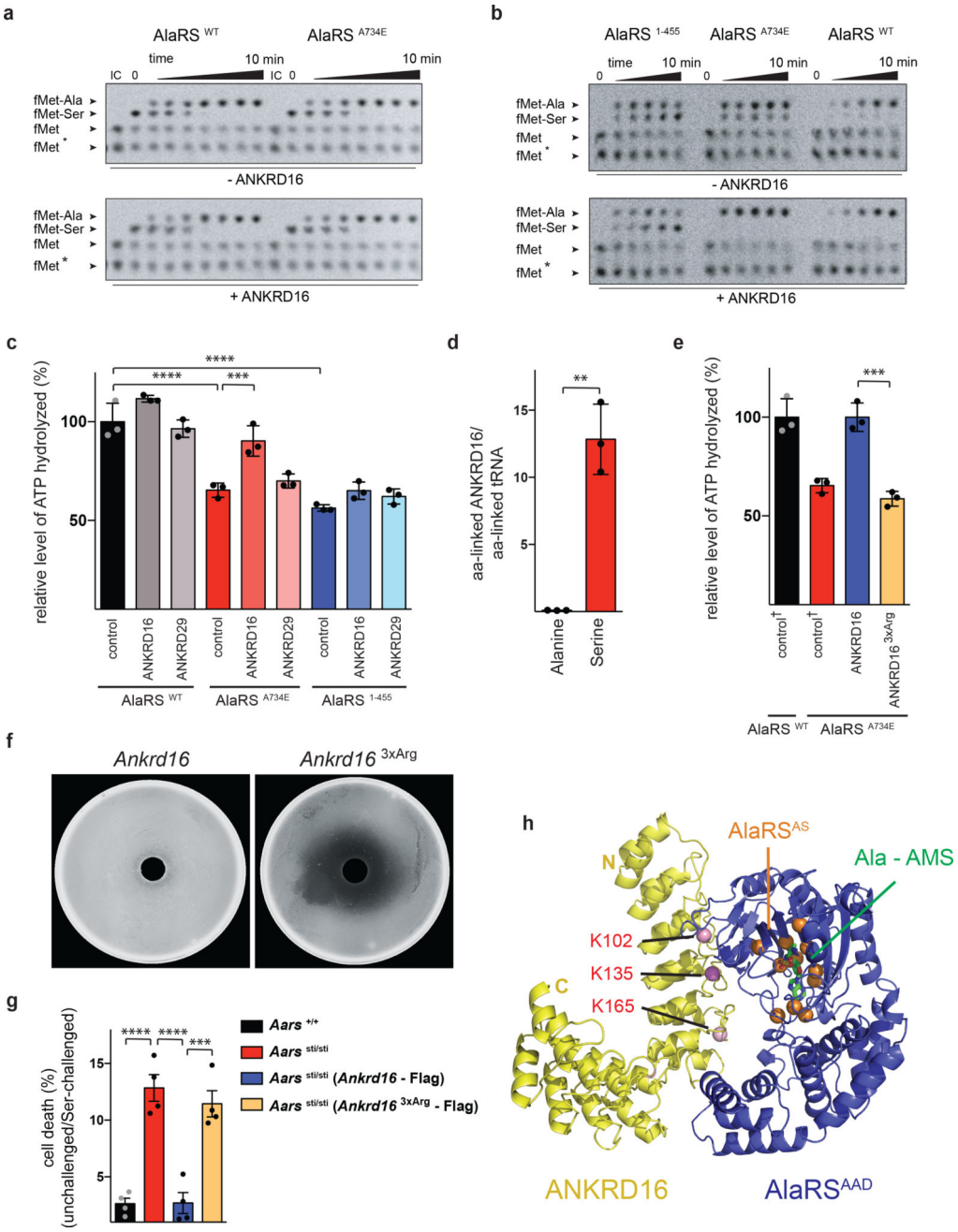

Figure 4. ANKRD16 enhances tRNA-independent editing and accepts serine adenylates from AlaRS

a, Mouse AlaRS (±ANKRD16) was added to reactions containing Ser-tRNA^{Ala} and alanine. **b,** Mouse AlaRS (±ANKRD16) was added to reactions containing deacylated tRNA^{Ala}, alanine and serine (* oxidized fMet). **c,** Ser-AMP hydrolysis at 10 min (mean ± SD, n = 3, One-way ANOVA (Tukey correction), *** $p \leq 0.001$, **** $p \leq 0.0001$). **d,** Ratio of alanine- or serine-linked ANKRD16/aminoacylated tRNA^{Ala} (mean ± SD, n = 3, Two-tailed Student's t-test, ** $p = 0.0011$). **e,** Ser-AMP hydrolysis at 10 min (mean ± SD, n = 3, One-way ANOVA (Tukey correction), *** $p \leq 0.001$). Control reactions from panel **c** (†). **f,**

Aars$^{C666A/Q584H}$ *E. coli* expressing mouse *Ankrd16* or *Ankrd16*^{3xArg}. **g,** Cell death of embryonic fibroblasts (mean ± SEM, n = 4, One-way ANOVA (Tukey correction), *** $p \leq 0.001$, **** $p \leq 0.0001$). **h,** Structural model of ANKRD16 and the aminoacylation domain (AAD) of AlaRS, modified lysines (purple), active site residues (orange), and Ala-AMS (Ala-AMP analog, green).

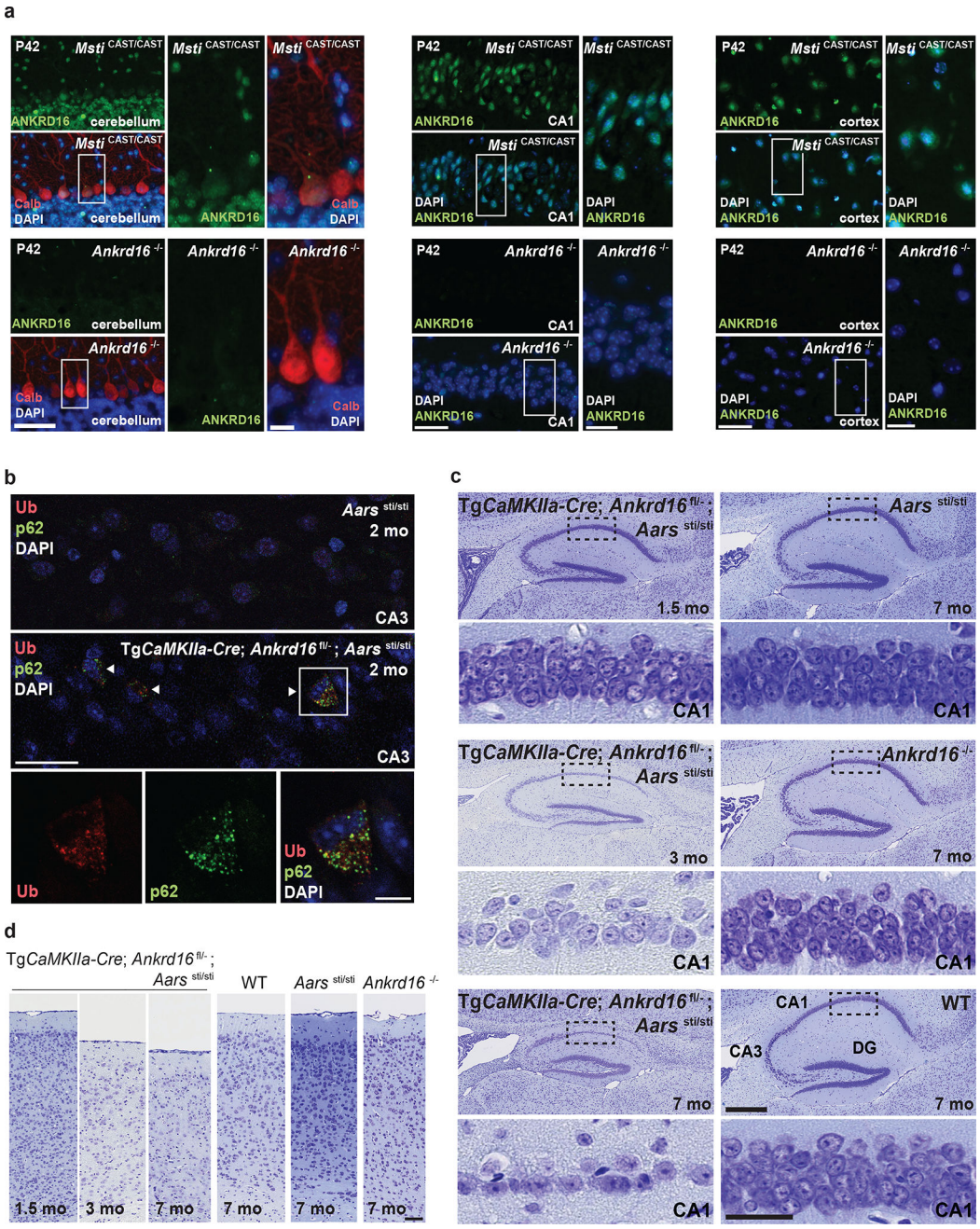

Figure 5. Loss of *Ankrd16* in *Aars*$^{sti/sti}$ mice causes protein aggregation and neurodegeneration

a and **b,** Immunofluorescence with antibodies to ANKRD16 (green) and calbindin D-28 (red) or ubiquitin (red) and p62 (green). **c** and **d,** Cresyl violet staining of hippocampus (**c**) and cortex (**d**). Scale bars: 50 μm (**a,** low magnification), 10 μm (**a,** higher magnification), 50 μm (**b**, low magnification), 10 μm (**b**, higher magnification), 500 μm (**c**, low magnification), 50 μm (**c**, higher magnification), 100 μm (**d**). Postnatal day (P), Cornu Ammonis (CA), Dentate gyrus (DG).